

Accurate Projection Methods for the Incompressible Navier–Stokes Equations

David L. Brown,^{*,1} Ricardo Cortez,^{†,2} and Michael L. Minion^{‡,3}

^{*}Center for Applied Scientific Computing, Lawrence Livermore National Laboratory, Livermore, California 94551; [†]Department of Mathematics, Tulane University, 6823 St. Charles Avenue, New Orleans, Louisiana 70118; and [‡]Department of Mathematics, Phillips Hall, CB 3250, University of North Carolina, Chapel Hill, North Carolina 27599

E-mail: dlb@llnl.gov, cortez@math.tulane.edu, minion@math.unc.edu

Received March 28, 2000; revised August 9, 2000

This paper considers the accuracy of projection method approximations to the initial–boundary-value problem for the incompressible Navier–Stokes equations. The issue of how to correctly specify numerical boundary conditions for these methods has been outstanding since the birth of the second-order methodology a decade and a half ago. It has been observed that while the velocity can be reliably computed to second-order accuracy in time and space, the pressure is typically only first-order accurate in the L_∞ -norm. This paper identifies the source of this problem in the interplay of the global pressure-update formula with the numerical boundary conditions and presents an improved projection algorithm which is fully second-order accurate, as demonstrated by a normal mode analysis and numerical experiments. In addition, a numerical method based on a gauge variable formulation of the incompressible Navier–Stokes equations, which provides another option for obtaining fully second-order convergence in both velocity and pressure, is discussed. The connection between the boundary conditions for projection methods and the gauge method is explained in detail. © 2001 Academic Press

Key Words: incompressible flow; projection method; boundary conditions.

¹The work of this author was performed under the auspices of the U.S. Department of Energy by University of California Lawrence Livermore National Laboratory and Los Alamos National Laboratory under Contracts W-7405-ENG-48 and W-7405-ENG-36.

²Supported in part by NSF Grant DMS-9816951.

³The work of this author was performed in part under the auspices of the U.S. Department of Energy by University of California Lawrence Livermore National Laboratory and Los Alamos National Laboratory under Contracts W-7405-ENG-48 and W-7405-ENG-36. Support also provided by the U.S. Department of Energy under Contract DE-FG02-92ER25139, NSF Grant DMS-9973290, and the Alfred P. Sloan Foundation.

1. INTRODUCTION

This paper considers the accuracy of projection method approximations to the initial-boundary-value problem for the incompressible Navier–Stokes equations. It is important to understand the behavior of such schemes since they form the basis not only for approximations to the equations that describe zero-Mach-number flows, but also for the equations describing low-Mach-number, possibly chemically reacting flows. In an n -dimensional bounded domain Ω , we consider the incompressible Navier–Stokes equations, written as

$$\mathbf{u}_t + \nabla p = -(\mathbf{u} \cdot \nabla)\mathbf{u} + \nu \nabla^2 \mathbf{u} \quad (1)$$

$$\nabla \cdot \mathbf{u} = 0 \quad (2)$$

with boundary conditions

$$\mathbf{u}|_{\partial\Omega} = \mathbf{u}_b, \quad (3)$$

where \mathbf{u} , the fluid velocity, and p , the pressure, are the “primitive variables,” and ν is the kinematic viscosity of the fluid.

Nearly all numerical methods for solving these equations in terms of the primitive variables use a fractional step approach. Some approximation to the momentum equation (1) is advanced to determine the velocity \mathbf{u} or a provisional velocity, and then an elliptic equation is solved that enforces the divergence constraint (2) and determines the pressure. In some variations, the viscous term in Eq. (1) is advanced in a separate step from the advective terms (e.g., [23]). Some methods solve directly for the pressure in the elliptic step (e.g., [19]); others solve for an auxiliary variable related to the pressure. Methods are often categorized as “pressure-Poisson” or “projection” methods based on which form of the elliptic constraint equation is being used. A distinguishing feature of the original projection method is that the velocity field is forced to satisfy a discrete divergence constraint at the end of each time step, while with pressure-Poisson methods, the velocity typically satisfies a discrete divergence constraint only to within the truncation error of the method. In recent years, projection methods which exactly enforce a discrete divergence constraint, or “exact” projection methods, have often been replaced with “approximate” projection methods (e.g., [3, 4, 26, 28]), which are similar to pressure-Poisson methods in that the velocity satisfies a discrete divergence constraint only to within the truncation error of the method. Approximate projection methods are used because of observed weak instabilities in exact methods (e.g., [25]) and the desire to use more complicated or adaptive finite difference meshes on which exact projections are difficult or mathematically impossible to implement [3, 28]. As a result, the mathematical differences between approximate projection and pressure-Poisson methods have become less clear; the practical differences between the two involve the number of fractional steps and the order in which they are taken. Additionally, as with all fractional step methods, a crucial issue is how boundary conditions are determined for some or all of the intermediate variables.

The determination of the fractional step equations and the intermediate boundary conditions in such a way as to obtain second- or higher-order convergence rates has been a subject of considerable discussion and interest over the past 20 years. This paper will focus on these issues for a particular class of projection methods that includes those introduced by Bell *et al.* [5, 6], Kim and Moin [24], and Van Kan [39]. These are of particular interest because

to date no variations of these methods that demonstrate completely second-order-in-time convergence in both the velocity and pressure variables for the viscous ($\nu > 0$) case have been published. Indeed, it has been observed both numerically and analytically that while second-order convergence in velocity can readily be obtained, the computed pressure is typically only first-order in time [16, 38]. There has even been speculation in the literature that these methods are inherently first-order in the pressure and cannot be improved to higher-order in the time variable [32, 36]. In this paper, we will demonstrate through normal mode analysis and numerical experiments that this class of projection methods can, in fact, be made fully second-order in time. The source of the problem lies in the interplay of the global pressure-update formula with the intermediate variable boundary conditions.

Projection methods pioneered by Chorin [9, 10] for numerically integrating (1,2,3) are based on the observation that the left-hand side of Eq. (1) is a Hodge decomposition. Hence an equivalent projection formulation is given by

$$\mathbf{u}_t = \mathbf{P}[-(\mathbf{u} \cdot \nabla)\mathbf{u} + \nu \nabla^2 \mathbf{u}], \quad (4)$$

where \mathbf{P} is the operator which projects a vector field onto the space of divergence-free vector fields with appropriate boundary conditions.

In the 1980s, several papers appeared in which second-order accurate versions of a projection method were proposed. Those of Goda [18], Bell *et al.* [5], Kim and Moin [24], and Van Kan [39] are motivated by the second-order, time-discrete semi-implicit forms of Eqs. (1) and (2),

$$\frac{\mathbf{u}^{n+1} - \mathbf{u}^n}{\Delta t} + \nabla p^{n+1/2} = -[(\mathbf{u} \cdot \nabla)\mathbf{u}]^{n+1/2} + \frac{\nu}{2} \nabla^2 (\mathbf{u}^{n+1} + \mathbf{u}^n) \quad (5)$$

$$\nabla \cdot \mathbf{u}^{n+1} = 0, \quad (6)$$

with boundary conditions

$$\mathbf{u}^{n+1}|_{\partial\Omega} = \mathbf{u}_b^{n+1}, \quad (7)$$

where $[(\mathbf{u} \cdot \nabla)\mathbf{u}]^{n+1/2}$ represents a second-order approximation to the convective derivative term at time level $t^{n+1/2}$ which is usually computed explicitly. (The notation \mathbf{w}^n is used to represent an approximation to $\mathbf{w}(t^n)$, where $t^n = n\Delta t$.) This formulation is desirable because, depending on the form of $[(\mathbf{u} \cdot \nabla)\mathbf{u}]^{n+1/2}$, it can reduce or eliminate the dependence of the stability of the method on the magnitude of viscosity [27].

Spatially discretized versions of the coupled Eqs. (5) and (6) are cumbersome to solve directly. Therefore, a fractional step procedure can be used to approximate the solution of the coupled system by first solving an analog to Eq. (5) (without regard to the divergence constraint) for an intermediate quantity \mathbf{u}^* , and then projecting this quantity onto the space of divergence-free fields to yield \mathbf{u}^{n+1} . In general this procedure is given by

Step 1: Solve for the intermediate field \mathbf{u}^*

$$\frac{\mathbf{u}^* - \mathbf{u}^n}{\Delta t} + \nabla q = -[(\mathbf{u} \cdot \nabla)\mathbf{u}]^{n+1/2} + \frac{\nu}{2} \nabla^2 (\mathbf{u}^* + \mathbf{u}^n), \quad (8)$$

$$B(\mathbf{u}^*) = 0, \quad (9)$$

where q represents an approximation to $p^{n+1/2}$ and $B(\mathbf{u}^*)$ a boundary condition for \mathbf{u}^* which must be specified as part of the method.

Step 2: Perform the projection

$$\mathbf{u}^* = \mathbf{u}^{n+1} + \Delta t \nabla \phi^{n+1} \tag{10}$$

$$\nabla \cdot \mathbf{u}^{n+1} = 0, \tag{11}$$

using boundary conditions consistent with $B(\mathbf{u}^*) = 0$ and $\mathbf{u}^{n+1}|_{\partial\Omega} = \mathbf{u}_b^{n+1}$.

Step 3: Update the pressure

$$p^{n+1/2} = q + L(\phi^{n+1}), \tag{12}$$

where the function L represents the dependence of $p^{n+1/2}$ on ϕ^{n+1} . Once the time step is completed, the predicted velocity \mathbf{u}^* is discarded, not to be used again at that or later time steps. We will refer to methods of this type generically as *incremental-pressure projection methods* since the projection step serves to compute an incremental-pressure gradient correction.

There are three choices that need to be made in the design of such a method. They are the pressure approximation q , the boundary condition $B(\mathbf{u}^*)$, and the function $L(\phi^{n+1})$ in the pressure-update equation. In this paper we explain the coupling among these three functions that must be considered for the overall method to be second-order accurate. In the process we show that several existing methods fall short of second-order accuracy up to the boundary precisely because this coupling was not considered.

An important issue is that the boundary condition for \mathbf{u}^* must be consistent with Eq. (10), although at the time the boundary conditions are applied the function ϕ^{n+1} is not yet known and hence must be approximated. The degree to which the gradient term must be approximated depends on the choice of q . One may speculate that, in the first step of the method, if q is a good approximation to $p^{n+1/2}$, the field \mathbf{u}^* may not differ significantly from the fluid velocity and thus a reasonable choice for the boundary condition $B(\mathbf{u}^*) = 0$ may be $(\mathbf{u}^* - \mathbf{u}_b)|_{\partial\Omega} = 0$. On the other hand, one may not be interested in computing the pressure at every time step and would like to choose $q = 0$ and obviate the third step in the method. In this case \mathbf{u}^* may differ significantly from the fluid velocity, requiring the boundary condition $B(\mathbf{u}^*)$ to include a nontrivial approximation of $\nabla\phi^{n+1}$ in Eq. (10). Later in the paper we make these statements precise and show the required degree of the approximations involved.

Regarding the third step of the method, substituting Eq. (10) into Eq. (8), eliminating \mathbf{u}^* , and comparing with Eq. (5) yield a formula for the pressure-update

$$p^{n+1/2} = q + \phi^{n+1} - \frac{\nu\Delta t}{2} \nabla^2 \phi^{n+1}, \tag{13}$$

which appeared (in gradient form) in [40]. The last term of this equation plays an important role in computing the correct pressure gradient and allows the pressure to retain second-order accuracy up to the boundary. Without this term, the pressure gradient may have zeroth-order accuracy at the boundary even if the pressure itself is high-order accurate. The normal mode analysis for the Stokes equations in Section 4 predicts second-order accuracy for both \mathbf{u} and p using Eq. (13). In particular, the analysis shows that spurious modes in the pressure, which

are present in some methods, are eliminated by the use of this improved pressure-update formula. Numerical experiments presented in Section 6 confirm these findings.

To fully understand how boundary conditions for projection methods should be chosen, it is helpful to consider an alternative formulation of the incompressible Navier–Stokes equations based on a variable first introduced by Oseledets [30]. This formulation is variously known as a “magnetization,” “impulse,” or “gauge” formulation. Numerical methods based on various forms of these variables have been developed by Buttke [8], and more recently by Cortez [12, 13], E and Liu [15, 17], Recchioni and Russo [34], and Summers and Chorin [37]. The numerical method based on these variables in this paper is essentially the same as the one proposed by E and Liu [15, 17]; hence we will refer to it as the gauge method.

Two new variables, \mathbf{m} and χ , are introduced that are related to the fluid velocity by

$$\mathbf{m} = \mathbf{u} + \nabla\chi. \quad (14)$$

The vector field \mathbf{m} and the potential χ can be chosen to satisfy evolution equations in such a way that the fluid velocity and pressure derived from them satisfy the Navier–Stokes equations. Given \mathbf{m} , one possibility, which is proposed in [17], is to let \mathbf{m} satisfy in Ω the evolution equation

$$\mathbf{m}_t + (\mathbf{u} \cdot \nabla)\mathbf{u} = \nu \nabla^2 \mathbf{m} \quad (15)$$

$$\mathbf{u}|_{\partial\Omega} = \mathbf{u}_b, \quad (16)$$

where

$$\mathbf{u} = \mathbf{P}(\mathbf{m}). \quad (17)$$

Equations (14)–(17) constitute an equivalent formulation of the Navier–Stokes Eqs. (1)–(3). In this formulation, the pressure has been eliminated from the equations; however, it can be recovered from the potential χ by enforcing the equivalence of Eqs. (1) and (15), giving

$$p = \chi_t - \nu \nabla^2 \chi. \quad (18)$$

Note that the boundary conditions are given in terms of \mathbf{u} , which by Eq. (14), implies that there is a coupling of the boundary conditions of \mathbf{m} and $\nabla\chi$.

A time-discrete form of the Eqs. (15) and (17) is given by

$$\frac{\mathbf{m}^{n+1} - \mathbf{m}^n}{\Delta t} = -[(\mathbf{u} \cdot \nabla)\mathbf{u}]^{n+1/2} + \frac{\nu}{2} \nabla^2 (\mathbf{m}^{n+1} + \mathbf{m}^n) \quad (19)$$

$$\mathbf{u}^{n+1} = \mathbf{m}^{n+1} - \nabla\chi^{n+1}, \quad (20)$$

where Eq. (20) is again the Hodge decomposition formulation of the projection. This is the second-order version of the gauge method presented by E and Liu in [15] and used by those authors in their numerical experiments. The pressure is not required in order to advance the velocity, although for some problems an accurate representation of the pressure at every

time step might be desired. If needed, the pressure can be computed from χ through the second-order approximation to Eq. (18)

$$p^{n+1/2} = \frac{\chi^{n+1} - \chi^n}{\Delta t} - \frac{\nu}{2} \nabla^2 (\chi^{n+1} + \chi^n). \tag{21}$$

Note that this method is very similar to the projection method of Kim and Moin described in Section 2.2, except that the variable \mathbf{m} is retained as a prognostic variable, rather than discarded at the end of each time step. The similarity is not superficial, for if initially $\mathbf{m} = \mathbf{u}$ (and hence $\nabla \chi = 0$), then the first time step of this method is identical to that of Kim and Moin with \mathbf{u}^* taking the place of \mathbf{m} , although of course the methods differ at later times.

The boundary conditions in Eq. (16) are written in terms of the velocity, but solving Eq. (19) requires boundary conditions for \mathbf{m}^{n+1} , which must satisfy Eq. (20) as a compatibility condition. There is some freedom in choosing these boundary conditions and the analysis in Section 4 predicts second-order convergence for both \mathbf{u} and p when the compatibility condition is satisfied. Numerical experiments indicating second-order accuracy for \mathbf{u} appear in [15]. The results in Section 6 show second-order accuracy for \mathbf{u} , p , and ∇p as well.

In Section 3, a detailed presentation will be provided of the boundary conditions required in the momentum and projection equations of the projection and gauge methods described before. The relationship between the boundary conditions for projection and gauge methods will become clear in the course of the presentation. In Section 4, a normal mode analysis of the methods as applied to the Stokes equations is performed in order to draw conclusions about the accuracy of the methods. In contrast to similar analyses performed previously, we consider general choices of q , $B(\mathbf{u}^*)$, and L (outlined earlier) to deduce the necessary conditions for second-order accuracy. In particular, the analysis shows that second-order accuracy in both the velocity and the pressure are obtainable with the correct choice of boundary conditions and pressure-update equations. It also shows that the formula traditionally used for the pressure-update leads to a decrease in the pressure accuracy. Finally, careful numerical studies of the methods when applied to the full incompressible Navier–Stokes equations are presented to substantiate the analysis.

2. COMMENTS ON SOME EXISTING METHODS

In this section we make brief comments about some of the methods mentioned earlier viewed in the context established in the Introduction. The purpose is not to review the literature but to describe the extent to which these methods are consistent with Eqs. (8)–(12) and the implications for their accuracy. We also comment on reported results that have contributed to the debate on the topic.

2.1. Bell, Colella, and Glaz

A well-known projection method is that of Bell *et al.* [5, 6], which has been applied in various settings and extended to more complicated physical problems such as reacting flows [1, 4, 6, 25, 26, 28]. In the typical implementation of this method [6], the predicted velocity \mathbf{u}^* is computed using Eqs. (8) and (9) with the choices $q = p^{n-1/2}$ and $B(\mathbf{u}^*) = (\mathbf{u}^* - \mathbf{u}_b^{n+1})|_{\partial\Omega} = 0$. The advection term is computed using a Godunov procedure. The projection step is performed by solving an elliptic problem for ϕ^{n+1} with the boundary

condition

$$\hat{\mathbf{n}} \cdot \nabla \phi^{n+1}|_{\partial\Omega} = 0, \quad (22)$$

which follows from the choice of $B(\mathbf{u}^*)$ and Eq. (10). We demonstrate later in this paper that for this method, \mathbf{u}^* differs at most by $\mathcal{O}(\Delta t^2)$ from the correct velocity \mathbf{u}^{n+1} , justifying the use of the velocity boundary condition for \mathbf{u}^* . The method produces solutions that converge in the maximum norm at a second-order rate for the velocity.

The pressure, however, converges at only a first-order rate. This is due to the pressure gradient update, given by

$$\nabla p^{n+1/2} = \nabla p^{n-1/2} + \nabla \phi^{n+1}, \quad (23)$$

which differs from Eq. (13) since the last term of the latter is not included. This omission results in lower accuracy for p and an inaccurate pressure gradient at the boundary. This is evident by noting that Eq. (22) and the normal component of Eq. (23) imply that $\hat{\mathbf{n}} \cdot \nabla p^{n+1/2} = \hat{\mathbf{n}} \cdot \nabla p^{n-1/2}$, for all n , which cannot be correct in general.

This loss of accuracy in the pressure, which typically manifests itself as a boundary layer, is well known and has been analyzed rigorously by Temam [38], E and Liu [16], Shen [35], and others. It is also asserted in [32, 36] that pressure-increment projection methods are inherently first-order in the pressure variable. This is true if the pressure-update in Eq. (23) is used, but the simple modification to the pressure increment equation, given in Eq. (13), recovers full second-order accuracy in the pressure.

2.2. Kim and Moin

The relationship between ϕ and p in Eq. (13) was recognized by Kim and Moin in [24], although the method they propose does not use a pressure gradient update. Instead, a fractional step discretization to Eq. (4) is used resulting in a method in which the pressure does not appear at all (i.e., $q = 0$ in Eq. (8)). We refer to methods of this type as *pressure-free projection methods*.

The absence of the pressure gradient term in the momentum equation for \mathbf{u}^* has two consequences. First, it could be considered appealing since it prohibits errors in the pressure gradient, which could accumulate in time, from contributing to errors in the momentum equation. Second, it implies that \mathbf{u}^* is no longer within $\mathcal{O}(\Delta t^2)$ of \mathbf{u}^{n+1} , and a nontrivial approximation of the gradient term in Eq. (10) is required when specifying a boundary condition for \mathbf{u}^* . Kim and Moin recognized this fact and argued that applying $\mathbf{u}^* = \mathbf{u}^{n+1} + \Delta t \nabla \phi^n$ at the boundary (i.e. approximating the unknown function ϕ^{n+1} with the previous value ϕ^n) is sufficient to obtain second-order accuracy in the velocities. Later, we show using normal mode analysis that this is also a necessary condition for second-order accuracy for this method.

Although the pressure is not required in order to advance the velocity, the authors in [24] mention the relation $p = \phi - (\nu \Delta t / 2) \nabla^2 \phi$. This must be interpreted as the time-centered pressure

$$p^{n+1/2} = \phi^{n+1} - \frac{\nu \Delta t}{2} \nabla^2 \phi^{n+1} \quad (24)$$

to be consistent with the second-order Crank–Nicolson method. If both the pressure and ϕ are evaluated at the same time level (i.e., if the right-hand side of Eq. (24) is set equal to p^{n+1}), the resulting pressure is only first-order accurate, as reported by Strikwerda and Lee [36]. We demonstrate in Section 4 that $p^{n+1/2}$ in Eq. (24) approximates the pressure at $t^{n+1/2}$ with second-order accuracy in time.

2.3. Botella, Perot, Hugues, and Randriamampianina

Although the following three methods are not analyzed in the normal mode analysis or numerical results in this paper, they have similar characteristics to the projection methods mentioned above. Botella [7] and Perot [32] both propose methods that reduce the truncation error associated with the computation of ∇p in the momentum equation by adding additional correction terms to the basic method. The second-order method proposed by Perot uses $q = 0$ and replaces the pressure-update formula (12) with

$$\left(I + \frac{\nu \Delta t}{2} \nabla^2 \right) p^{n+1/2} = \phi^{n+1}. \tag{25}$$

This method still only obtains first-order convergence in the pressure since $\hat{\mathbf{n}} \cdot \nabla p = 0$ is the boundary condition used for the elliptic pressure equation.

Botella proposes using a third-order integration formula for the evaluation of the time derivative in the momentum equation although this does not affect the truncation error associated with the pressure term. In the present context, a second-order version of Botella’s method would use

$$q = p^{n-1/2} + \phi^n, \tag{26}$$

which is in fact a time extrapolation of the pressure, while the projection-update (10) would be

$$\mathbf{u}^{n+1} = \mathbf{u}^* - \Delta t \nabla (\phi^{n+1} - \phi^n), \tag{27}$$

and the pressure-update equation

$$p^{n+1/2} = p^{n-1/2} + \phi^{n+1}. \tag{28}$$

Botella is able to demonstrate higher-order convergence for the velocity and the pressure in an L^2 norm, although it is apparent from the pressure-update formula (28) that with this method, $\hat{\mathbf{n}} \cdot \nabla p$, must stay constant, and hence inaccurate, on the boundary if $\hat{\mathbf{n}} \cdot \nabla \phi = 0$ is used as a boundary condition for the projection step.

Hugues and Randriamampianina [22] recognized that using a pressure-update equation such as Eq. (28) results in an inconsistent normal pressure gradient at boundaries. To avoid this, they proposed a second-order method using an Adams–Bashforth/BDF semi-implicit method in time in which a Poisson problem is first solved for the provisional pressure gradient appearing in the momentum equation. The right side and boundary conditions for the Poisson equation are extrapolated in time. Hence, in the present context, q would be found by the solution of an additional Poisson problem. The provisional pressure is then updated with an equation analogous to Eq. (28). We speculate that an additional term in the pressure-update analogous to Eq. (13) would lead to a more accurate pressure for this method.

2.4. *E and Liu*

E and Liu [15] have used the method described in Eq. (19), in which the boundary condition for \mathbf{m}^{n+1} was given by Eq. (20) with the term χ^{n+1} approximated by $2\chi^n - \chi^{n-1}$. This idea of extrapolating boundary values was used previously by Karniadakis *et al.* [23] to approximate the pressure boundary condition in the context of a pressure-Poisson method. E and Liu demonstrate that their method is second-order for \mathbf{u} and ϕ . Here we demonstrate second-order convergence in numerical tests for p and ∇p and demonstrate that extrapolation in time is in fact necessary for this accuracy; i.e., using only a lagged value χ^n leads to first-order accuracy. The projection method results reported in [15] were obtained using the traditional pressure update of Eq. (23), which should lead to a reduced order of accuracy in p . A loss in accuracy in the velocities is also reported which is attributed to the approximate projection employed. Here we demonstrate that full second-order accuracy in all variables can be calculated using an approximate projection without any special spatial differencing (at least in the simple geometry considered).

3. BOUNDARY CONDITIONS

The numerical methods presented in the last section require the solution of implicit equations for which boundary conditions must be imposed. Besides the implicit momentum Eqs. (8) and (19), the implementation of a projection also requires a boundary condition. The choice of these boundary conditions will now be discussed. For ease of presentation, the equations will be considered in two dimensions only. Extensions to three dimensions are straightforward.

The most common way in which a projection \mathbf{P} is specified is by the solution of a Poisson equation. Specifically, let $\mathbf{w} = \mathbf{v} + \nabla\phi$ be the Hodge decomposition of \mathbf{w} , where \mathbf{v} is divergence-free and required to satisfy $\mathbf{v}|_{\partial\Omega} = \mathbf{v}_b$ (by the divergence theorem \mathbf{v}_b must satisfy $\int_{\partial\Omega} \mathbf{v}_b = 0$). Then to find \mathbf{v} from \mathbf{w} we let

$$\mathbf{v} = \mathbf{P}(\mathbf{w}) = \mathbf{w} - \nabla\phi,$$

where

$$\begin{aligned} \nabla^2\phi &= \nabla \cdot \mathbf{w} \\ \hat{\mathbf{n}} \cdot \nabla\phi|_{\partial\Omega} &= \hat{\mathbf{n}} \cdot (\mathbf{w}|_{\partial\Omega} - \mathbf{v}_b). \end{aligned} \tag{29}$$

It is important to note that the projection \mathbf{P} as defined implies that \mathbf{v} automatically satisfies the normal boundary condition $\hat{\mathbf{n}} \cdot \mathbf{v}|_{\partial\Omega} = \hat{\mathbf{n}} \cdot \mathbf{v}_b$, but the tangential condition $\hat{\mathbf{t}} \cdot \mathbf{v}|_{\partial\Omega} = \hat{\mathbf{t}} \cdot \mathbf{v}_b$ will only be satisfied if \mathbf{w} is such that $\hat{\mathbf{t}} \cdot \mathbf{w}|_{\partial\Omega} = \hat{\mathbf{t}} \cdot (\mathbf{v}_b + \nabla\phi|_{\partial\Omega})$. This is a critical observation that impacts the choice of boundary conditions for Eqs. (8) and (19), since in each case, the projection of the solution of this equation is expected to satisfy both normal and tangential boundary conditions.

Consider first the gauge method in Eqs. (19) and (20). Suppose we arbitrarily set the boundary conditions for the momentum equation in terms of \mathbf{m} to be

$$\mathbf{m}^{n+1}|_{\partial\Omega} = \mathbf{m}_b^{n+1}, \tag{30}$$

for some \mathbf{m}_b^{n+1} . We now consider choosing boundary conditions in the elliptic equation for χ^{n+1} in such a way that the updated velocity will satisfy $\mathbf{u}^{n+1}|_{\partial\Omega} = \mathbf{u}_b$. Unfortunately, this is not possible since the elliptic problem accepts only one boundary condition; e.g.,

$$\hat{\mathbf{n}} \cdot \nabla \chi^{n+1}|_{\partial\Omega} = \hat{\mathbf{n}} \cdot (\mathbf{m}_b^{n+1} - \mathbf{u}_b^{n+1}).$$

By the compatibility constraint $\mathbf{u}^{n+1} = \mathbf{m}^{n+1} - \nabla \chi^{n+1}$, the normal component of the updated velocity will be correct. The tangential component of \mathbf{u}^{n+1} , on the other hand, will satisfy

$$\hat{\mathbf{t}} \cdot \mathbf{u}^{n+1}|_{\partial\Omega} = \hat{\mathbf{t}} \cdot (\mathbf{m}_b^{n+1} - \nabla \chi^{n+1}|_{\partial\Omega}),$$

which can only be correct if \mathbf{m}_b^{n+1} had been chosen originally to satisfy

$$\hat{\mathbf{t}} \cdot \mathbf{m}_b^{n+1} = \hat{\mathbf{t}} \cdot (\mathbf{u}_b^{n+1} + \nabla \chi^{n+1}|_{\partial\Omega}).$$

This equation involves χ^{n+1} , which is unknown at the time \mathbf{m}_b^{n+1} must be set, and hence is the discrete manifestation of the coupling between the boundary conditions for \mathbf{m} and $\nabla \chi$ mentioned in the Introduction. Although unknown, $\nabla \chi^{n+1}$ can be approximated by extrapolating the values from previous time steps as proposed by E and Liu [15]. In the next section it is shown that this extrapolation is *necessary* for the resulting velocity and pressure to be second-order accurate in the maximum norm.

Next consider the boundary conditions for the pressure-free projection method in Eq. (8) with the choice $q = 0$. As mentioned before, one step of the pressure-free method is identical to the first time step of the gauge method if $\nabla \chi$ is initially set to zero with \mathbf{u}^* taking the place of \mathbf{m} . Hence it becomes clear how one might treat the boundary conditions in such a projection method. Specifically, in the boundary condition $B(\mathbf{u}^*)$, the normal piece $\hat{\mathbf{n}} \cdot \mathbf{u}^*$ appears to be arbitrary since the normal boundary condition on \mathbf{u}^{n+1} is implied by the projection. A convenient choice is $\hat{\mathbf{n}} \cdot \mathbf{u}^*|_{\partial\Omega} = \hat{\mathbf{n}} \cdot \mathbf{u}_b^{n+1}$ since by Eq. (29), it implies homogeneous Neumann boundary conditions for ϕ^{n+1} in the subsequent projection. However, since the necessity for a boundary condition for \mathbf{u}^* arises from the parabolic nature of Eq. (8), one can imagine that the choice of boundary condition for \mathbf{u}^* will affect the nature of the function \mathbf{u}^* near the boundary. Since, by Eq. (24), the pressure is determined from

$$p^{n+1/2} = \phi^{n+1} - \frac{\nu}{2} \nabla \cdot \mathbf{u}^*, \quad (31)$$

the behavior of the pressure near the boundary will also be affected by the choice of this boundary condition. Indeed, as discussed in Section 6.4, we observe in numerical experiments that unless the boundary condition for \mathbf{u}^* is chosen in such a way as to keep \mathbf{u}^* smooth up to the boundary, the pressure may not be recovered to $\mathcal{O}(\Delta t^2)$ by this method. The situation for the tangential boundary condition for \mathbf{u}^* is clearer. This boundary condition must be chosen so that when \mathbf{u}^* is projected to yield \mathbf{u}^{n+1} , the tangential boundary condition on \mathbf{u}^{n+1} is satisfied.

In [24] a Taylor series argument is used to show that using a lagged value of ϕ in the boundary condition $\hat{\mathbf{t}} \cdot \mathbf{u}^*|_{\partial\Omega} = \hat{\mathbf{t}} \cdot (\mathbf{u}_b^{n+1} + \Delta t \nabla \phi^n|_{\partial\Omega})$ is enough to ensure second-order accuracy. It is also possible to estimate $\nabla \phi^{n+1}|_{\partial\Omega}$ more accurately by extrapolation in time. The continuity of $\nabla \phi$ in time is implied by the fact that \mathbf{u}^* satisfies an elliptic equation with continuous forcing and $\Delta t \nabla \phi$ is simply $(\mathbf{I} - \mathbf{P})\mathbf{u}^*$.

Finally, consider the momentum equation (8) with the choice $q = p^{n-1/2}$. Again there is some freedom in choosing the boundary value for $\hat{\mathbf{n}} \cdot \mathbf{u}^*$ since the projection will ensure that $\hat{\mathbf{n}} \cdot \mathbf{u}^{n+1}|_{\partial\Omega} = \hat{\mathbf{n}} \cdot \mathbf{u}_b^{n+1}$. Since in this case the goal is to have \mathbf{u}^* be a good approximation to \mathbf{u}^{n+1} , the correct choice is $\hat{\mathbf{t}} \cdot \mathbf{u}^*|_{\partial\Omega} = \hat{\mathbf{t}} \cdot \mathbf{u}_b^{n+1}$. As before, the tangential piece should satisfy $\hat{\mathbf{t}} \cdot \mathbf{u}^*|_{\partial\Omega} = \hat{\mathbf{t}} \cdot (\mathbf{u}_b^{n+1} + \Delta t \nabla \phi^{n+1}|_{\partial\Omega})$, but if \mathbf{u}^* is a good approximation to \mathbf{u}^{n+1} , then $\hat{\mathbf{t}} \cdot \nabla \phi^{n+1}|_{\partial\Omega}$ may be negligibly small and $\hat{\mathbf{t}} \cdot \mathbf{u}^*|_{\partial\Omega} = \hat{\mathbf{t}} \cdot \mathbf{u}_b^{n+1}$ should suffice. A simple Taylor series argument along the lines of that in [24] can be used to show that \mathbf{u}^{n+1} is a second-order accurate approximation to \mathbf{u}^* at the boundary [40]. Another possibility is to use a lagged value of $\nabla \phi$ as in the Kim and Moin scheme or to extrapolate in time. These choices will be analyzed in detail in the following section.

4. NORMAL MODE ANALYSIS

The original Dirichlet problem as stated in Eqs. (1)–(3) requires only a condition on the velocity \mathbf{u} on the boundary. In two dimensions, this consists of two scalar conditions which can be thought of as conditions on the normal and tangential components of the velocity. As discussed in the previous section, for the fractional step methods considered in this paper, three boundary conditions are required, two for the implicit momentum equation and one for the projection. The purpose of this section is to establish the impact of various boundary condition possibilities on the overall accuracy of semi-implicit methods for gauge and projection formulations for the incompressible Navier–Stokes equations. In particular, necessary conditions for second-order accuracy are developed.

4.1. Reference Solution

It is most convenient to analyze the accuracy of these methods by using normal mode analysis (see, e.g., [14–16, 20, 21, 23, 29, 36]). Since the essential details we are concerned with result from the interaction of the boundary conditions with the Crank–Nicolson time stepping of the viscous terms, the advective derivative term can be neglected, and we can therefore consider the simpler problem of the unsteady Stokes equations in the periodic semiinfinite strip $\Omega = [0, \infty) \times [-\pi, \pi]$, for $t \geq 0$. This domain was considered in [36] and makes the analysis easier than a channel with two boundaries. The unsteady Stokes equations in primitive variables are given by

$$\begin{aligned} \mathbf{u}_t &= -\nabla p + \nu \nabla^2 \mathbf{u} \\ \nabla \cdot \mathbf{u} &= 0 \end{aligned} \tag{32}$$

and are considered with boundary conditions

$$u(0, y, t) = \alpha, \quad v(0, y, t) = \beta.$$

By taking the divergence of the Stokes equation, one derives an elliptic equation for the pressure; the resulting system requires the additional condition that the velocity divergence is zero on the boundary [9, 21, 29]:

$$\begin{aligned} \mathbf{u}_t &= -\nabla p + \nu \nabla^2 \mathbf{u} \quad \text{in } \Omega \\ \nabla^2 p &= 0 \quad \text{in } \Omega \\ u(0, y, t) &= \alpha, \quad v(0, y, t) = \beta, \quad \nabla \cdot \mathbf{u} = 0 \quad \text{on } \partial\Omega. \end{aligned} \tag{33}$$

$$u(0, y, t) = \alpha, \quad v(0, y, t) = \beta, \quad \nabla \cdot \mathbf{u} = 0 \quad \text{on } \partial\Omega. \tag{34}$$

Taking the Fourier transform in y and the Laplace transform in t leads to the equivalences $\partial_t \rightarrow s$ and $\partial_y \rightarrow ik$. Denoting transformed variables with hats, the previous equations become

$$\begin{aligned} v(-\partial_x^2 + \mu^2)\hat{u} &= -\partial_x \hat{p} \\ v(-\partial_x^2 + \mu^2)\hat{v} &= -ik\hat{p} \\ (-\partial_x^2 + k^2)\hat{p} &= 0, \end{aligned} \tag{35}$$

where k is the wavenumber in the y -direction, s is the Laplace transform variable, and μ is the root with positive real part of $\mu^2 = k^2 + s/v$. Bounded solutions of Eq. (34) take the form

$$\begin{aligned} \hat{u} &= Ue^{-\mu x} + \frac{|k|}{s}Pe^{-|k|x} \\ \hat{v} &= Ve^{-\mu x} - \frac{ik}{s}Pe^{-|k|x} \\ \hat{p} &= Pe^{-|k|x}. \end{aligned} \tag{36}$$

The undetermined constants U , V , and P are found by applying the boundary conditions in Eq. (34), which leads to the system

$$\begin{pmatrix} 1 & 0 & |k|/s \\ 0 & 1 & -ik/s \\ -\mu & ik & 0 \end{pmatrix} \begin{pmatrix} U \\ V \\ P \end{pmatrix} = \begin{pmatrix} \hat{\alpha} \\ \hat{\beta} \\ 0 \end{pmatrix}, \tag{37}$$

whose solution is given by

$$\begin{aligned} U &= \frac{v(\mu + |k|)}{s}(-|k|\hat{\alpha} + ik\hat{\beta}) \\ V &= \frac{-iv(\mu + |k|)\mu}{s}\left(-\frac{k}{|k|}\hat{\alpha} + i\hat{\beta}\right) \\ P &= \frac{v(\mu + |k|)}{|k|}(\mu\hat{\alpha} - ik\hat{\beta}). \end{aligned} \tag{38}$$

The functional form of the solution is then given by

$$\begin{aligned} \hat{u} &= \frac{v(\mu + |k|)}{s}(-|k|\hat{\alpha} + ik\hat{\beta})e^{-\mu x} + \frac{v(\mu + |k|)}{s}(\mu\hat{\alpha} - ik\hat{\beta})e^{-|k|x} \\ \hat{v} &= \frac{v(\mu + |k|)}{s}\left(\frac{i\mu k}{|k|}\hat{\alpha} + \mu\hat{\beta}\right)e^{-\mu x} - \frac{v(\mu + |k|)}{s}\frac{k}{|k|}(i\mu\hat{\alpha} + k\hat{\beta})e^{-|k|x} \\ \hat{p} &= \frac{v(\mu + |k|)}{|k|}(\mu\hat{\alpha} - ik\hat{\beta})e^{-|k|x}. \end{aligned} \tag{39}$$

This will be used as the reference or “true” solution in the discussion that follows.

4.2. *The Gauge Method*

In [15], E and Liu present a normal mode analysis for their first-order version of the gauge method. In this section, we consider the second-order-in-time formulation and include in the analysis the extrapolation of the boundary values of χ . Let $\mathbf{m} = (m_1, m_2)$ and consider a method of the form

$$\begin{aligned} \frac{\mathbf{m}^{n+1} - \mathbf{m}^n}{\Delta t} &= \frac{\nu}{2} \nabla^2 (\mathbf{m}^{n+1} + \mathbf{m}^n) \\ \nabla^2 \chi^{n+1} &= \nabla \cdot \mathbf{m}^{n+1} \\ \mathbf{u}^{n+1} &= \mathbf{m}^{n+1} - \nabla \chi^{n+1}, \end{aligned} \tag{40}$$

with boundary conditions at $x = 0$ given by

$$\begin{aligned} m_1^{n+1} &= \gamma \\ m_2^{n+1} &= \beta + \partial_y \tilde{\chi} \\ \partial_x \chi^{n+1} &= \gamma - \alpha, \end{aligned} \tag{41}$$

where $\partial_y \tilde{\chi}$ is an approximation to $\partial_y \chi^{n+1}$. The first two boundary conditions are imposed on the momentum equation, and the last boundary condition is used with the elliptic equation for χ . If $\partial_y \chi^{n+1}$ were known before the elliptic problem was solved, then one would expect to recover the correct solution.

As before, taking the Fourier and Laplace transforms and denoting $\kappa = e^{s\Delta t}$ leads to the system

$$\begin{aligned} (-\partial_x^2 + \bar{\mu}^2) \hat{m}_1 &= 0 \\ (-\partial_x^2 + \bar{\mu}^2) \hat{m}_2 &= 0 \\ (-\partial_x^2 + k^2) \hat{\chi} &= -\partial_x \hat{m}_1 - ik \hat{m}_2, \end{aligned} \tag{42}$$

where $\bar{\mu}^2 = k^2 + \rho/\nu$, with $\rho = 2(\kappa - 1)/\Delta t(\kappa + 1) = s + \mathcal{O}(s^3 \Delta t^2)$. Note also that therefore $\bar{\mu} = \mu + \mathcal{O}(s^2 \Delta t^2)$. The solution has the form

$$\begin{aligned} \hat{m}_1 &= A e^{-\bar{\mu}x} \\ \hat{m}_2 &= B e^{-\bar{\mu}x} \\ \hat{\chi} &= \frac{1}{\rho} (P e^{-|k|x} - \bar{\mu} \nu \hat{m}_1 + ik \nu \hat{m}_2). \end{aligned} \tag{43}$$

For the boundary condition involving $\tilde{\chi}$ one could use a lagged value $\tilde{\chi} = \chi^n$ or the second-order extrapolation formula $\tilde{\chi} = 2\chi^n - \chi^{n-1}$. In either case one arrives at the system

$$\begin{pmatrix} \bar{\mu}^2 \nu & -ik \bar{\mu} \nu & -|k| \\ ik \bar{\mu} \nu & k^2 \nu + C \rho & -ik \\ 1 & 0 & 0 \end{pmatrix} \begin{pmatrix} A \\ B \\ P \end{pmatrix} = \begin{pmatrix} \rho(\hat{\gamma} - \hat{\alpha}) \\ C \rho \hat{\beta} \\ \hat{\gamma} \end{pmatrix}, \tag{44}$$

where $C = \kappa = 1 + \mathcal{O}(s \Delta t)$ when $\tilde{\chi} = \chi^n$ and $C = \kappa^2 / (2\kappa - 1) = 1 + \mathcal{O}(s^2 \Delta t^2)$ with the extrapolation formula.

Solving the system for A , B , and P and setting $\hat{u} = \hat{m}_1 - \partial_x \hat{\chi}$ and $\hat{v} = \hat{m}_2 - ik\hat{\chi}$ yields

$$\hat{u} = \frac{\nu(\mu + |k|)}{\rho}(-|k|\hat{\alpha} + ik\hat{\beta})e^{-\mu x} + \frac{\nu(\mu + |k|)}{\rho}(\mu\hat{\alpha} - ik\hat{\beta})e^{-|k|x} + \mathcal{O}(C - 1)$$

$$\hat{v} = \frac{\nu(\mu + |k|)}{\rho} \left(\frac{i\mu k}{|k|}\hat{\alpha} + \mu\hat{\beta} \right) e^{-\mu x} - \frac{\nu(\mu + |k|)}{\rho} \frac{k}{|k|}(i\mu\hat{\alpha} + k\hat{\beta})e^{-|k|x} + \mathcal{O}(C - 1).$$

Observing that $\rho = s + \mathcal{O}(s^3 \Delta t^2)$, it follows that the reference solution is recovered to $\mathcal{O}(\Delta t^2)$ as long as the extrapolated boundary condition for χ is used. Using a lagged boundary value $\tilde{\chi} = \chi^n$ would result in an $\mathcal{O}(\Delta t)$ approximation. Also note that using the pressure Eq. (21) leads to

$$\hat{p} = \frac{\nu(\mu + |k|)}{|k|}(\mu\hat{\alpha} - ik\hat{\beta})e^{-|k|x} + \mathcal{O}(C - 1).$$

Thus the gauge method with extrapolated boundary conditions is overall a second-order accurate method.

4.3. Projection Methods

In order to obtain an accurate solution to the incompressible Navier–Stokes equations using the projection methods described by Eqs. (8)–(12), one either must devise a procedure for accurately approximating the boundary conditions $\mathbf{u}^* - \Delta t \nabla \phi = (\alpha, \beta)^T$ or reformulate the problem in such a way that \mathbf{u}^* is a sufficiently accurate approximation to \mathbf{u} . In the latter case, the boundary conditions $\mathbf{u}^* = (\alpha, \beta)^T$ will then be accurate approximations to the original conditions $\mathbf{u} = (\alpha, \beta)^T$, and one expects to obtain overall accuracy in the method. In a general formulation of the projection methods described before, the momentum equation is given by

$$\frac{\mathbf{u}^* - \mathbf{u}^n}{\Delta t} + \nabla q = \frac{\nu}{2} \nabla^2 (\mathbf{u}^n + \mathbf{u}^*), \tag{45}$$

where ∇q is related to the pressure. The velocity satisfies $\nabla \cdot \mathbf{u}^{n+1} = 0$ and is given by

$$\mathbf{u}^{n+1} = \mathbf{u}^* - \Delta t \nabla \phi^{n+1} \tag{46}$$

and the pressure is updated with

$$p^{n+1/2} = q + L\phi^{n+1}, \tag{47}$$

where L is a linear differential operator.

Referring to Eqs. (8), (10), and (12), three combinations of q and L will be considered:

1. a projection method similar to that of Bell, Colella, and Glaz, described by $q = p^{n-1/2}$ and $L = I$. This combination will be referred to as projection method I (PmI),
2. a similar projection method that uses the improved pressure-update formula Eq. (13). This combination corresponds to $q = p^{n-1/2}$ and $L = I - \frac{\nu \Delta t}{2} \nabla^2$ and will be referred to as PmII,
3. a projection method similar to that of Kim and Moin’s, which corresponds to $q = 0$ and $L = I - \frac{\nu \Delta t}{2} \nabla^2$. This method will be referred to as PmIII.

For the normal mode analysis, we first eliminate the variable \mathbf{u}^* by substituting Eq. (46) into Eq. (45) to get

$$\frac{\mathbf{u}^{n+1} - \mathbf{u}^n}{\Delta t} + \nabla \phi^{n+1} + \nabla q = \frac{\nu}{2} \nabla^2 (\mathbf{u}^{n+1} + \mathbf{u}^n) + \frac{\nu \Delta t}{2} \nabla^2 \nabla \phi^{n+1}.$$

After taking Fourier and Laplace transforms, let $\kappa = e^{s\Delta t}$ and define $\hat{\phi}$ by

$$\hat{q} = \kappa^{n+1} Q(\kappa) \hat{\phi}, \quad (48)$$

where $Q(\kappa)$ depends on the choice of q in Eq. (45) and L in Eq. (47). This leads to

$$(-\partial_x^2 + \bar{\mu}^2) \hat{\mathbf{u}} = -\frac{\kappa \Delta t}{\kappa + 1} (-\partial_x^2 + \lambda^2) \nabla \hat{\phi} - \frac{2\kappa Q(\kappa)}{\nu(\kappa + 1)} \nabla \hat{\phi}, \quad (49)$$

where $\bar{\mu}$ and λ are defined by

$$\bar{\mu}^2 = k^2 + \rho/\nu, \quad \rho = \frac{2(\kappa - 1)}{\Delta t(\kappa + 1)}, \quad \lambda^2 = k^2 + \frac{2}{\nu \Delta t}. \quad (50)$$

Taking the divergence of Eq. (49) leads to the equation for $\hat{\phi}$

$$\left[-\partial_x^2 + \lambda^2 + \frac{2Q(\kappa)}{\nu \Delta t} \right] (-\partial_x^2 + k^2) \hat{\phi} = 0$$

so that $\hat{\phi}$ can be written as $\hat{\phi} = \hat{\phi}_1 + \hat{\phi}_2$ where

$$(-\partial_x^2 + k^2) \hat{\phi}_1 = 0, \quad \left[-\partial_x^2 + \lambda^2 + \frac{2Q(\kappa)}{\nu \Delta t} \right] \hat{\phi}_2 = 0. \quad (51)$$

We note that $\hat{\phi}_1$ contains the piece of the solution that we expect to have; however, $\hat{\phi}_2$ represents a spurious mode in the potential $\hat{\phi}$, which should not appear in the velocities or the pressure. It is easy to show that $\hat{\mathbf{u}}$ does not contain this spurious mode. This can be seen by writing $\hat{\phi}$ on the right-hand side of Eq. (49) as the sum of $\hat{\phi}_1$ and $\hat{\phi}_2$ and noticing from Eq. (51) that $Q(\kappa) \hat{\phi}_2 = -\frac{\nu \Delta t}{2} (-\partial_x^2 + \lambda^2) \hat{\phi}_2$. All terms with $\hat{\phi}_2$ drop out, resulting in the equation

$$(-\partial_x^2 + \bar{\mu}^2) \hat{\mathbf{u}} = -\frac{2\kappa(1 + Q(\kappa))}{\nu(\kappa + 1)} \nabla \hat{\phi}_1,$$

from which we deduce the following form for the solutions:

$$\hat{\phi} = A_1 e^{-|k|x} + \hat{\phi}_2 \quad (52)$$

$$\hat{u} = U e^{-\bar{\mu}x} + \frac{2\kappa(1 + Q(\kappa))}{\rho(\kappa + 1)} |k| A_1 e^{-|k|x} \quad (53)$$

$$\hat{v} = V e^{-\bar{\mu}x} - \frac{2\kappa(1 + Q(\kappa))}{\rho(\kappa + 1)} i k A_1 e^{-|k|x}. \quad (54)$$

From Eqs. (47) and (48) we find that the pressure is given by

$$\hat{p} = \kappa^{1/2} (Q(\kappa) + L) \hat{\phi}. \quad (55)$$

The last equation and the choice of q determine the operator $Q(\kappa)$ and $\hat{\phi}_2$.

For example, in PmI, where $q = p^{n-1/2}$ and $L = I$, we have that

$$\kappa^{n+1} Q(\kappa)\hat{\phi} = \hat{q} = \kappa^{n-1/2}\hat{p} = \kappa^n(Q(\kappa) + L)\hat{\phi},$$

from which we find that $Q(\kappa) = \frac{1}{\kappa-1}$ and $\hat{\phi}_2 = A_2 e^{-\tilde{\lambda}x}$, where $\tilde{\lambda}^2 = k^2 + \frac{2\kappa}{v\Delta t(\kappa-1)}$. In view of Eq. (55) this implies that the pressure is given by

$$\hat{p} = \frac{\kappa^{3/2}}{\kappa-1}\hat{\phi},$$

which contains the spurious mode.

On the other hand, consider PmII, where $q = p^{n-1/2}$, $L = I - \frac{v\Delta t}{2}\nabla^2$, and hence $L\hat{\phi} = \frac{v\Delta t}{2}(-\partial_x^2 + \lambda^2)\hat{\phi}$. Now we have that

$$Q(\kappa)\hat{\phi} = \frac{L\hat{\phi}}{\kappa-1} = \frac{v\Delta t}{2(\kappa-1)}(-\partial_x^2 + \lambda^2)\hat{\phi},$$

which implies that $\hat{\phi}_2 = A_2 e^{-\lambda x}$ and

$$\hat{p} = \frac{\kappa^{3/2}}{\kappa-1}L\hat{\phi} = \frac{\kappa^{3/2}}{\kappa-1}A_1 e^{-|k|x},$$

so that the pressure does not contain the spurious mode $\hat{\phi}_2$.

PmIII uses $q = 0$ and $L = I - \frac{v\Delta t}{2}\nabla^2$. In this case $Q(\kappa) \equiv 0$ so that $\hat{\phi}_2 = A_2 e^{-\lambda x}$ and $\hat{p} = \kappa^{1/2}L\hat{\phi} = \kappa^{1/2}\frac{v\Delta t}{2}(-\partial_x^2 + \lambda^2)\hat{\phi}$, which is again the operator that eliminates the spurious mode.

Considering Eqs. (52)–(54), all of the methods discussed here lead to

$$\hat{\phi} = A_1 e^{-|k|x} + A_2 e^{-\gamma x} \tag{56}$$

$$\hat{u} = U e^{-\bar{\mu}x} + R(\kappa)\frac{|k|}{\rho}A_1 e^{-|k|x} \tag{57}$$

$$\hat{v} = V e^{-\bar{\mu}x} - R(\kappa)\frac{ik}{\rho}A_1 e^{-|k|x}, \tag{58}$$

where the variables $R(\kappa)$, γ , and $F(\kappa)$, related by

$$R(\kappa) = \frac{2\kappa(1 + Q(\kappa))}{(1 + \kappa)} \quad \text{and} \quad \gamma^2 = k^2 + \frac{2}{v\Delta t}F(\kappa),$$

depend on the method.

4.3.1. The boundary conditions. For the normal mode analysis of the projection methods, the following boundary conditions are applied,

$$u^* = \alpha, \quad \phi_x = 0, \quad v^* = \beta + \Delta t \tilde{\phi}_y, \quad \text{and} \quad u_x + v_y = 0, \tag{59}$$

where $\tilde{\phi}$ is an approximation to ϕ^{n+1} . Three choices for $\tilde{\phi}$ are considered:

$$\tilde{\phi} = 0 \Leftrightarrow \text{zeroth order}$$

$$\tilde{\phi} = \phi^n \Leftrightarrow \text{first order}$$

$$\tilde{\phi} = 2\phi^n - \phi^{n-1} \Leftrightarrow \text{second order.}$$

After transformation, the boundary conditions in Eq. (59) become

$$\hat{u} = \hat{\alpha}, \quad \hat{\phi}_x = 0, \quad \hat{v} + ik\Delta t B(\kappa)\hat{\phi} = \hat{\beta}, \quad \text{and} \quad \hat{u}_x + ik\hat{v} = 0, \quad (60)$$

where $B(\kappa)$ equals 1, $(\kappa - 1)/\kappa$, or $(\kappa - 1)^2/\kappa^2$ depending on the choice of $\tilde{\phi}$.

4.3.2. *Solving for the coefficients.* Since the boundary condition $\hat{\phi}_x = 0$ simply implies that $\gamma A_2 = -|k|A_1$, and $\hat{u}_x + ik\hat{v} = 0$ implies $ikV = \bar{\mu}U$, we focus on determining the coefficients U and A_1 . Inserting the boundary conditions into Eqs. (56)–(58) and eliminating V and A_2 lead to the equations

$$\begin{aligned} \bar{\mu}U + k^2 \left[\frac{R(\kappa)}{\rho} - \frac{2F(\kappa)B(\kappa)}{v\gamma(\gamma + |k|)} \right] A_1 &= ik\hat{\beta} \\ U + R(\kappa) \frac{|k|}{\rho} A_1 &= \hat{\alpha} \end{aligned}$$

from which we find that

$$A_1 = \frac{v(\bar{\mu} + |k|)(\bar{\mu}\hat{\alpha} - ik\hat{\beta})}{|k|R(\kappa)} \left[1 + C \frac{F(\kappa)B(\kappa)}{R(\kappa)} \right]^{-1} \quad (61)$$

$$U = \left[\frac{v(\bar{\mu} + |k|)(ik\hat{\beta} - \hat{\alpha}|k|)}{\rho} + \hat{\alpha}C \frac{F(\kappa)B(\kappa)}{R(\kappa)} \right] \left[1 + C \frac{F(\kappa)B(\kappa)}{R(\kappa)} \right]^{-1} \quad (62)$$

$$V = -\frac{i\bar{\mu}}{k}U \quad (63)$$

$$A_2 = -\frac{|k|}{\gamma}A_1, \quad (64)$$

where

$$C = \frac{2|k|(\bar{\mu} + |k|)}{\gamma(\gamma + |k|)}.$$

The accuracy of this solution is considered next.

4.3.3. *Results.* Since $\rho = s + \mathcal{O}(s^3\Delta t^2)$, it is clear that for the solution corresponding to the coefficients in Eqs. (61)–(64) to be within $\mathcal{O}(\Delta t^2)$ of the reference solution (38), the term

$$C \frac{F(\kappa)B(\kappa)}{R(\kappa)}$$

must be $\mathcal{O}(\Delta t^2)$. This represents the coupling between the pressure gradient approximation in the momentum equation and the boundary conditions. The choice of q and the pressure-update operator L determine $F(\kappa)$ and $R(\kappa)$, while the boundary conditions determine $B(\kappa)$.

One can use the fact that $\gamma(\gamma + |k|) \geq \gamma^2 = \frac{2F(\kappa) + k^2v\Delta t}{v\Delta t}$ to show that

$$C \frac{F(\kappa)B(\kappa)}{R(\kappa)} \leq 2|k|v(\bar{\mu} + |k|) \frac{\Delta t B(\kappa)F(\kappa)}{R(\kappa)[2F(\kappa) + k^2v\Delta t]}.$$

Therefore it is sufficient to show that

$$\frac{B(\kappa)F(\kappa)}{R(\kappa)[2F(\kappa) + k^2\nu\Delta t]} = \mathcal{O}(\Delta t).$$

First consider the term $R(\kappa)$ which also appears in the denominator of A_1 . For PmI and PmII (when $q = p^{n-1/2}$), one would expect ϕ to be at least as small as $\mathcal{O}(\Delta t)$. For PmIII, where $q = 0$, one would expect ϕ to be $\mathcal{O}(1)$. (Notice that in Eq. (46), $\nabla\phi^{n+1}$ appears with a factor Δt .) This is confirmed by recalling that $R(\kappa) = 2\kappa(1 + Q(\kappa))/(1 + \kappa)$, so that

$$q = p^{n-1/2} \Leftrightarrow R(\kappa) = \frac{2\kappa^2}{\kappa - 1} \sim \mathcal{O}(\Delta t^{-1})$$

$$q = 0 \Leftrightarrow R(\kappa) = \frac{2\kappa}{\kappa + 1} \sim \mathcal{O}(1).$$

By examining the size of the remaining terms, the following results are evident:

- PmI uses $q = p^{n-1/2}$ and $L = I$. This leads to $F(\kappa) = \frac{\kappa}{\kappa-1}$ and

$$\frac{B(\kappa)F(\kappa)}{R(\kappa)[2F(\kappa) + k^2\nu\Delta t]} \sim B(\kappa) \mathcal{O}(\Delta t).$$

Therefore it is only necessary that $B(\kappa) = \mathcal{O}(1)$, which allows the use of the boundary condition $v^* = \beta$ (corresponding to $\tilde{\phi} = 0$). However, as explained before, the pressure is given by

$$\hat{p} = \frac{\kappa^{3/2}}{\kappa - 1} \hat{\phi},$$

which includes the coefficient of the spurious mode $\frac{\kappa^{3/2}}{\kappa-1} A_2 \sim \mathcal{O}(\nu\Delta t)$. Thus, the expected convergence rate for the velocities is $\mathcal{O}(\Delta t^2)$, while the pressure is only expected to be first order in time with this method.

- For PmII, which uses $q = p^{n-1/2}$ and the improved pressure-update formula $L = I - \frac{\nu\Delta t}{2}\nabla^2$, we have that $F(\kappa) = 1$ and

$$\frac{B(\kappa)F(\kappa)}{R(\kappa)[2F(\kappa) + k^2\nu\Delta t]} \sim B(\kappa) \mathcal{O}(\Delta t)$$

as before. Again, it is sufficient to use $v^* = \beta$ as a boundary condition. In this case the pressure is given by

$$p = \frac{\kappa^{3/2}}{\kappa - 1} L\phi,$$

which removes the spurious mode. For this method, both the velocities u, v and the pressure p are expected to converge to second order in time.

- For PmIII with $q = 0$ and $L = I - \frac{\nu\Delta t}{2}\nabla^2$ again $F = 1$, but

$$\frac{B(\kappa)F(\kappa)}{R(\kappa)[2F(\kappa) + k^2\nu\Delta t]} \sim B(\kappa) \mathcal{O}(1).$$

It is therefore required that $B(\kappa) = \mathcal{O}(\Delta t)$ for second-order accuracy. Hence the boundary condition $v^* = \beta + \Delta t \tilde{\phi}_y$ must use at least the lagged value $\tilde{\phi} = \phi^n$. This is true regardless of the choice of the pressure-update operator L since the pressure is not needed to advance the solution. The operator L only affects the pressure (if one were to compute it) since $p = \kappa^{1/2} L\phi$. So if $L = I$ then p will contain the spurious mode $\gamma = \lambda$ resulting in $\mathcal{O}(v\Delta t)$ errors. If $L = I - \frac{v\Delta t}{2} \nabla^2$ then p will not contain the spurious mode and will be second-order accurate in time, as will be the velocity components u and v .

5. THE NUMERICAL METHODS

This section describes the numerical methods that will be applied to the full Navier–Stokes equations. Most of the motivation for the form of the numerical methods can be inferred from the earlier sections of the paper; hence only the details are presented here.

In the following, all the spatial differential operators with a subscript h are assumed to be centered second-order discrete approximations to the continuous counterparts. In all the numerical methods, the time-centered advective derivative $[(\mathbf{u} \cdot \nabla_h)\mathbf{u}]^{n+1/2}$ is computed using second-order centered differences in space and second-order extrapolation in time [24].

5.1. The Gauge Method

The following method is essentially the second-order gauge method proposed by E and Liu in [15]. Equation (15) is discretized using the second-order, semiimplicit formula

$$\frac{\mathbf{m}^{n+1} - \mathbf{m}^n}{\Delta t} = -[(\mathbf{u} \cdot \nabla_h)\mathbf{u}]^{n+1/2} + \frac{\nu}{2} \nabla_h^2 (\mathbf{m}^n + \mathbf{m}^{n+1}). \tag{65}$$

The boundary conditions, consistent with the compatibility condition $(\mathbf{m}^{n+1} - \nabla \chi^{n+1})|_{\partial\Omega} = \mathbf{u}_b^{n+1}$, are

$$\begin{aligned} \hat{\mathbf{n}} \cdot \mathbf{m}^{n+1}|_{\partial\Omega} &= \mathbf{n} \cdot \mathbf{u}_b^{n+1} \\ \hat{\mathbf{t}} \cdot \mathbf{m}^{n+1}|_{\partial\Omega} &= \hat{\mathbf{t}} \cdot \mathbf{u}_b^{n+1} + \hat{\mathbf{t}} \cdot \nabla_h (2\chi^n - \chi^{n-1})|_{\partial\Omega}. \end{aligned}$$

The velocity at the end of the time step is defined by

$$\mathbf{u}^{n+1} = \mathbf{m}^{n+1} - \nabla_h \chi^{n+1}, \tag{66}$$

where χ^{n+1} is the solution of

$$\nabla_h^2 \chi^{n+1} = \nabla_h \cdot \mathbf{m}^{n+1} \quad \text{in } \Omega \tag{67}$$

$$\hat{\mathbf{n}} \cdot \nabla \chi^{n+1} = 0 \quad \text{on } \partial\Omega. \tag{68}$$

If needed, the pressure is computed with Eq. (21):

$$p^{n+1/2} = \frac{\chi^{n+1} - \chi^n}{\Delta t} - \frac{\nu}{2} \nabla_h^2 (\chi^{n+1} + \chi^n). \tag{69}$$

5.2. Projection Methods with a Lagged Pressure Term

The method first described in this section is referred to as PmI. It is similar to the method developed by Bell *et al.* [5, 6], except in the treatment of the advective derivatives which are computed as in [24] with a second-order Adams–Bashforth formula.

The first step of the projection method is found by solving

$$\frac{\mathbf{u}^* - \mathbf{u}^n}{\Delta t} + \nabla p^{n-1/2} = -[(\mathbf{u} \cdot \nabla_h)\mathbf{u}]^{n+1/2} + \frac{\nu}{2}\nabla_h^2(\mathbf{u}^n + \mathbf{u}^*) \quad (70)$$

for the intermediate field \mathbf{u}^* with boundary conditions

$$\mathbf{u}^* = \mathbf{u}_b^{n+1}.$$

Next, \mathbf{u}^{n+1} is recovered from the projection of \mathbf{u}^* by solving

$$\Delta t \nabla_h^2 \phi^{n+1} = \nabla_h \cdot \mathbf{u}^* \quad \text{in } \Omega \quad (71)$$

$$\hat{\mathbf{n}} \cdot \nabla_h \phi^{n+1} = 0 \quad \text{on } \partial\Omega \quad (72)$$

and setting $\mathbf{u}^{n+1} = \mathbf{u}^* - \Delta t \nabla_h \phi^{n+1}$.

The new pressure is computed as in [6, 39] by

$$\nabla_h p^{n+1/2} = \nabla_h p^{n-1/2} + \nabla_h \phi^{n+1}. \quad (73)$$

As discussed before, this formula is not consistent with a second-order discretization of the Navier–Stokes equations since, due to Eq. (72), the normal component of the pressure gradient will remain constant in time at the boundary.

A second implementation of the method just described can be made by utilizing the correct pressure update given by Eq. (13). Specifically, Eqs. (70)–(72) are used in combination with

$$\nabla_h p^{n+1/2} = \nabla_h p^{n-1/2} + \nabla_h \phi^{n+1} - \frac{\nu \Delta t}{2} \nabla_h \nabla_h^2 \phi^{n+1}. \quad (74)$$

This form of the projection method is projection method II (PmII).

5.3. A Projection Method without Pressure Gradient

The method presented in this section is referred to as PmIII. It is similar to the method of Kim and Moin [24], but uses a different spatial discretization and a slightly different treatment of the boundary conditions. The momentum equation is discretized by

$$\frac{\mathbf{u}^* - \mathbf{u}^n}{\Delta t} = -[(\mathbf{u} \cdot \nabla_h)\mathbf{u}]^{n+1/2} + \frac{\nu}{2}\nabla_h^2(\mathbf{u}^n + \mathbf{u}^*) \quad (75)$$

and we first consider boundary conditions

$$\begin{aligned} \hat{\mathbf{n}} \cdot \mathbf{u}^*|_{\partial\Omega} &= \hat{\mathbf{n}} \cdot \mathbf{u}_b^{n+1} \\ \hat{\mathbf{t}} \cdot \mathbf{u}^*|_{\partial\Omega} &= \hat{\mathbf{t}} \cdot (\mathbf{u}_b^{n+1} + \Delta t \nabla_h \phi^n)|_{\partial\Omega}. \end{aligned}$$

As before, $\mathbf{u}^{n+1} = \mathbf{P}(\mathbf{u}^*)$; i.e., $\mathbf{u}^{n+1} = \mathbf{u}^* - \Delta t \nabla_h \phi^{n+1}$, where ϕ^{n+1} satisfies Eqs. (71) and (72).

The pressure-update equation is now

$$\nabla_h p^{n+1/2} = \nabla_h \phi^{n+1} - \frac{\nu \Delta t}{2} \nabla_h \nabla_h^2 \phi^{n+1}, \quad (76)$$

which is Eq. (74) without the term $\nabla p^{n-1/2}$.

5.4. Additional Numerical Details

The numerical implementation of the projections used in the methods requires that a Poisson problem be solved (see the beginning of Section 3). In these problems, the Laplacian is approximated with a standard five-point stencil and the divergence and gradient with second-order centered differences. This combination produces an approximate rather than an exact projection operator in the sense that projected velocities only satisfy a discrete divergence constraint to truncation error [4]. Approximate projection methods have become increasingly popular in recent years, but the ramifications of using approximate projections are not well understood, although some work has been done for the case of inviscid flow without boundaries [2].

Since the test problems studied in the next section are all set in a periodic channel, the inversion of the Laplacian in the projection is made efficient by first taking the discrete Fourier transform of the equation in the x -direction. This results in N one-dimensional linear systems which are solved with a direct method. The system corresponding to the zeroth wave number is singular since the overall solution is determined only up to an arbitrary constant. This system is augmented with an additional constraint on the sum of unknowns (see [19] for details).

In the numerical methods presented above, extrapolation in time is used to compute the time-centered advective derivatives as well as the tangential boundary conditions for the implicit treatment of the momentum equation. Since these terms cannot be extrapolated at the first time step, an iterative procedure is employed. For example, for the gauge method the iteration can be written in two steps,

$$\begin{aligned} \frac{\mathbf{m}^{1,k} - \mathbf{m}^0}{\Delta t} &= -[(\mathbf{u} \cdot \nabla_h) \mathbf{u}]^{1/2,k} + \frac{\nu}{2} \nabla_h^2 (\mathbf{m}^0 + \mathbf{m}^{1,k}) \\ \hat{\mathbf{n}} \cdot \mathbf{m}^{1,k} &= \hat{\mathbf{n}} \cdot \mathbf{u}_b^1 \end{aligned}$$

and

$$\hat{\boldsymbol{\tau}} \cdot \mathbf{m}^{1,k} = \hat{\boldsymbol{\tau}} \cdot \nabla_h \chi^{1,k-1} + \hat{\boldsymbol{\tau}} \cdot \mathbf{u}_b^1 \quad \text{on } \partial\Omega$$

followed by

$$\begin{aligned} \nabla_h^2 \chi^{1,k} &= \nabla_h \cdot \mathbf{m}^{1,k} \\ \hat{\mathbf{n}} \cdot \nabla_h \chi^{1,k} &= 0 \quad \text{on } \partial\Omega. \end{aligned}$$

To begin, $\chi^{1,0} = \chi^0$. The advective derivative term is reset each iteration by taking the average of the derivatives of \mathbf{u}^0 and $\mathbf{u}^{1,k}$. The iteration for the projection method is done

in the analogous manner. The number of iterations is arbitrarily set to 5 for the first step and 2 for the second. This iterative procedure could be used at every time step rather than extrapolation, but at an additional computational cost.

For the projection method wherein the lagged pressure appears in the momentum equation, the initial pressure is used for this term in the first time step. It is calculated by solving the Poisson problem which results from taking the divergence of the momentum equation.

When calculating finite differences near solid wall boundaries, standard stencils cannot be used. When calculating $\nabla \cdot \mathbf{u}^*$ in the projection and the correction terms in the pressure-update equations, values of the particular differenced quantity are calculated at boundary points using quadratic extrapolation from the first three interior values. Since the explicit advective and diffusive terms in the momentum equation only appear at interior points in the right-hand side of the equation for \mathbf{u}^* or (\mathbf{m}^{n+1}) , these terms are not needed at the boundary.

A concern relating to the fact that the tangential component of the velocity boundary condition is not satisfied exactly remains to be addressed. For example, in projection method I, $\hat{\tau} \cdot \nabla_h \phi^{n+1}$ is not constrained at the boundary; hence

$$\hat{\tau} \cdot \mathbf{u}^{n+1}|_{\partial\Omega} = \hat{\tau} \cdot (\mathbf{u}_b^{n+1} - \Delta t \nabla_h \phi^{n+1})|_{\partial\Omega},$$

which is in error by $\Delta t \hat{\tau} \cdot \nabla_h \phi^{n+1}$. An analogous error occurs in each of the other methods. One way to address this is to simply reset the tangential component of velocity to the correct value at the end of each time step (see, e.g., Strikwerda and Lee [36]). Another choice is to simply let the values at the boundary remain as computed. A potential problem with using the first approach is that it could reduce the smoothness of \mathbf{u} increasing the error when explicit differences are taken at the points just inside the boundary (especially in the diffusive terms). For this reason a combination of both strategies is used here. Whenever derivatives which are normal to the boundary are calculated, the nonaltered form of the velocity is used; however, the tangential velocity itself is reset at the boundary after each time step. In the test problems presented, the alternative strategies produced similar results. A related discussion can be found in [33].

6. NUMERICAL RESULTS

In this section numerical examples are presented which confirm the validity of the normal mode analysis presented in Section 4 for the gauge and projection methods. Two problems are considered, one which uses an analytical forcing to yield an exact solution and one which is forced only by the motion of one boundary. The test problems are set in a channel with periodic boundary conditions in the x -direction and no-flow boundaries at $y = 0$ and $y = 1$. This geometry is the simplest setting in which to consider slip boundary conditions. A no-slip condition is prescribed at $y = 0$, while a nontrivial slip condition is specified at $y = 1$. Results from more complicated geometries will be reported in subsequent work.

In order for the temporal errors predicted in the normal mode analysis to be evident, the numerical experiments must be designed with the following considerations in mind.

1. The temporal errors should not be dominated by spatial error, therefore the problems considered use fine grids and smooth flows.
2. The pressure should have a nontrivial normal gradient at solid wall boundaries in the test problems chosen (as normally is the case in applications). If the normal pressure gradient

is compelled to remain zero by the application of a forcing term, then the inconsistency in the pressure gradient in projection method I and those in [5, 7, 32] cannot be distinguished.

3. Since the first-order temporal error terms for the pressure in the normal mode analysis are scaled by the viscosity, it is important that the viscosity be large enough compared to the grid size so that $\Delta x^2 \ll \nu \Delta t$.

4. The analysis is applicable to unsteady flow. The problems chosen have nontrivial spatial and temporal structure.

6.1. Forced Flow

In the first example, the Navier–Stokes equations are augmented with a forcing term in order for the solution to be

$$\begin{aligned} u &= \cos(2\pi(x - \omega(t)))(3y^2 - 2y) \\ v &= 2\pi \sin(2\pi(x - \omega(t)))y^2(y - 1) \\ p &= -\frac{\omega'(t)}{2\pi} \sin(2\pi(x - \omega(t)))(\sin(2\pi y) - 2\pi y + \pi) \\ &\quad - \nu \cos(2\pi(x - \omega(t)))(-2 \sin(2\pi y) + 2\pi y - \pi) \end{aligned}$$

with $\omega(t) = 1 + \sin(2\pi t^2)$. In terms of the gauge method variables, this solution corresponds to

$$\begin{aligned} m_1 &= \cos(2\pi(x - \omega(t)))(3y^2 - 2y) - \frac{1}{2\pi} \sin(2\pi(x - \omega(t)))(\sin(2\pi y) - 2\pi y + \pi) \\ m_2 &= 2\pi \sin(2\pi(x - \omega(t)))y^2(y - 1) + \frac{1}{2\pi} \cos(2\pi(x - \omega(t)))(\cos(2\pi y) - 1) \\ \phi &= \frac{1}{4\pi^2} \cos(2\pi(x - \omega(t)))(\sin(2\pi y) - 2\pi y + \pi). \end{aligned}$$

The viscosity is set to $\nu = 1$, which corresponds to a Reynolds number of 1 since the velocity is of unit magnitude. A uniform time step of $\Delta t = h/2$ is used corresponding to a CFL number of 1/2. Errors are calculated at time 0.5 in the both L_1 and L_∞ norms for $N \times N$ grids with N equal to 192, 256, and 384. The errors for the u -component of velocity are displayed in Table I which confirms that each method is producing second-order accurate solutions for u in both the L_1 and L_∞ norm. The results for v are similar and are not shown.

Next, the accuracy of the pressure is investigated. The normal mode analysis predicts that projection method I should display only first-order convergence in the pressure. The rest of the methods should be second-order accurate. Table II shows this to be the case. Note that the L_∞ norm of the error for projection method I is much larger than the L_1 norm. Figure 1 shows three profiles of the pressure error for projection method I from the 256×256 and 384×384 runs corresponding to values of $x = 3/16, 6/16, \text{ and } 9/16$. These profiles shows that the first-order error appears as boundary layer. The graphs show the error near the bottom boundary where no flow and no slip conditions are specified. Another boundary layer of similar shape and magnitude appears at the top of the domain.

TABLE I
Errors in the u -Component of Velocity for the Forced Flow Test Problem

		Errors in the u velocity			
		192×192	256×256	384×384	Rate
Gauge	L_1	1.46e-4	8.25e-5	3.68e-5	1.99
	L_∞	7.73e-4	4.44e-4	2.02e-4	1.94
PmI	L_1	7.53e-5	4.28e-5	1.91e-5	1.99
	L_∞	3.63e-4	2.13e-4	9.83e-5	1.90
PmII	L_1	7.25e-5	4.15e-5	1.87e-5	1.97
	L_∞	3.38e-4	2.01e-4	9.46e-5	1.86
PmIII	L_1	8.28e-5	4.67e-5	2.08e-5	1.99
	L_∞	3.38e-4	2.01e-4	9.46e-5	1.86

Note. The rates were computed from the errors in the 256×256 and 384×384 grids.

6.2. *Necessity for Accurate Boundary Conditions for $\hat{\tau} \cdot \mathbf{u}^*$*

One of the important results from the normal mode analysis is the required accuracy in the approximation of the tangential boundary condition for \mathbf{u}^* (or \mathbf{m}^{n+1} for the gauge method). To illustrate this, the forced flow problem was recomputed using a different tangential boundary condition for \mathbf{u}^* (or \mathbf{m}^{n+1}) for each method. The specific choices for the boundary conditions, as well as a summary of the errors which appear in Tables III and IV are contained in the points below.

- For the impulse method, the normal mode analysis predicts that $\hat{\tau} \cdot \nabla^{n+1}$ must be approximated with extrapolation to yield second-order accuracy. For this test, the lagged value $\hat{\tau} \cdot \nabla \chi^n$ is used instead, which results in a loss of accuracy in both the velocities and pressure.
- For projection method I, the usual boundary condition is $\hat{\tau} \cdot \mathbf{u}^* = 0$. For this test, the more accurate lagged value $\hat{\tau} \cdot \nabla \phi^n$ is used. Although this choice decreases the size of the errors somewhat, the order of the method is not changed. In particular, since the pressure is still updated using the inconsistent Eq. (23), the pressure is only first-order accurate near the boundary.

TABLE II
Errors the Pressure for the Forced Flow Test Problem

		Errors in the pressure			
		192×192	256×256	384×384	Rate
Gauge	L_1	2.57e-3	1.44e-3	6.40e-4	2.00
	L_∞	1.50e-2	8.47e-3	3.78e-3	1.99
PmI	L_1	2.91e-3	1.70e-3	7.83e-4	1.91
	L_∞	2.55e-2	1.73e-2	1.04e-2	1.26
PmII	L_1	1.55e-3	8.94e-4	4.07e-4	1.94
	L_∞	9.65e-3	5.56e-3	2.53e-3	1.94
PmIII	L_1	1.58e-3	9.15e-4	4.16e-4	1.94
	L_∞	1.09e-2	6.33e-3	2.94e-3	1.89

Note. The rates were computed from the errors in the 256×256 and 384×384 grids.

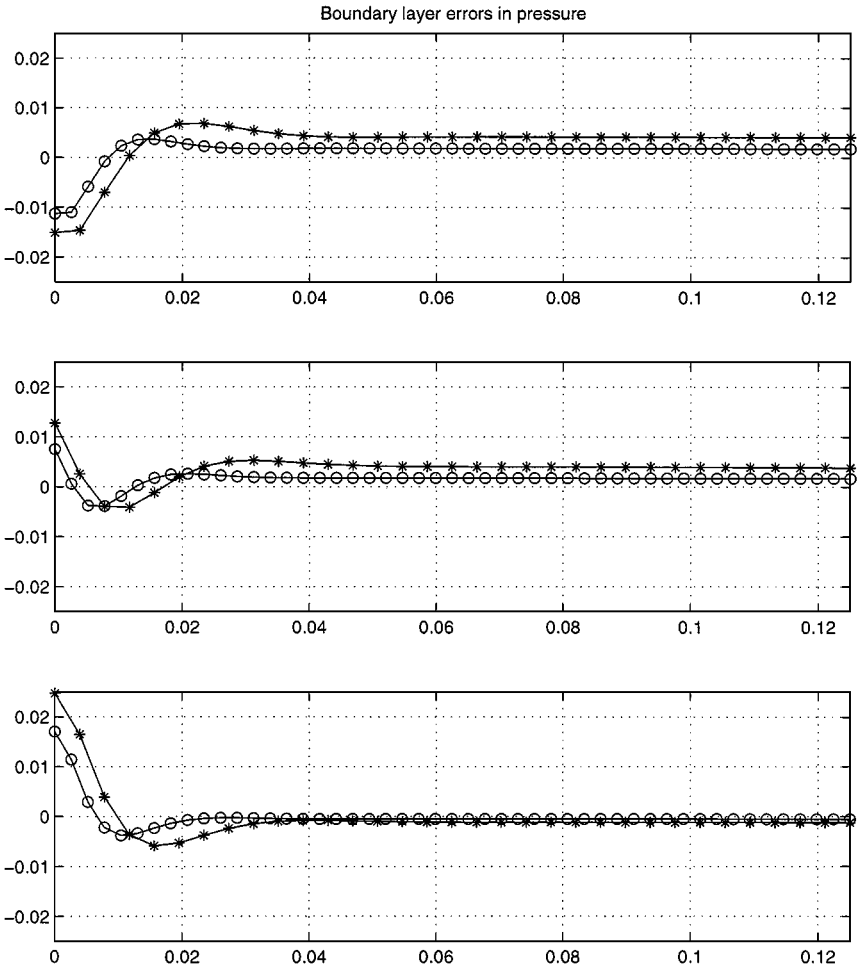


FIG. 1. First-order boundary layer error for projection method I. The three graphs correspond to profiles at x locations $3/16$, $6/16$, and $9/16$. Each graph shows the error from the 256×256 (*) and 384×384 (o) runs.

- The same lagged boundary condition as above can also be used for projection method II. Again this choice decreases the size of the errors somewhat, but the order of the method is not changed.

- For projection method III, the normal mode analysis indicates that using the lagged value $\hat{\tau} \cdot \nabla^n$ is necessary for second-order accuracy. For this test, the less accurate boundary condition $\hat{\tau} \cdot \mathbf{u}^* = 0$ was used (as is done normally done for PmII) which results in a loss of accuracy in both the velocities and the pressure. If the original boundary condition is made more accurate by extrapolation (as in the gauge method), the result is a reduction in the size but not the order of the errors, much the same as that observed for PmII above.

6.3. Unforced Flow

A second numerical experiment is now presented in which no forcing term is used. The same periodic channel geometry is used with zero boundary conditions at the bottom wall,

TABLE III
Errors in the u -Component of Velocity for the Forced Flow Test Problem When Different Boundary Extrapolations Are Used

		Errors in the u velocity			
		192 × 192	256 × 256	384 × 384	Rate
Gauge	L_1	3.67e-4	2.58e-4	1.61e-4	1.16
	L_∞	1.43e-3	9.76e-4	5.92e-4	1.23
PmI	L_1	4.84e-5	2.70e-5	1.19e-5	2.02
	L_∞	1.61e-4	9.09e-5	4.05e-5	1.99
PmII	L_1	4.70e-5	2.63e-5	1.16e-5	2.01
	L_∞	1.59e-4	8.97e-5	3.99e-5	2.00
PmIII	L_1	2.43e-3	1.87e-3	1.29e-3	0.92
	L_∞	2.26e-2	1.76e-2	1.22e-2	0.90

Note. The rates were computed from the errors in the 256 × 256 and 384 × 384 grids.

while no-flow and the slip condition $\hat{\tau} \cdot \mathbf{u}_b = e^{10r^2} - 1$ is imposed on the top wall. The initial conditions for the flow are given by

$$u = \sin(2\pi y) \sin^2(\pi x)$$

$$v = -\sin(2\pi x) \sin^2(\pi y).$$

For the gauge method, the initial condition $\mathbf{m} = \mathbf{u}$ is used and the boundary condition $\mathbf{m} \cdot \hat{\mathbf{n}} = 0$ is specified at both top and bottom boundaries throughout the computation.

Since no exact solution is known, a reference solution was computed on a 1152 × 1152 grid, and errors are estimated by the difference from this solution. To assure that the reference solution being used is valid, both the impulse method and PmII were used to compute the solution; it was observed that the maximum difference between the two solutions was 1.31×10^{-6} in the velocity, 2.23×10^{-6} in the pressure, and 8.73×10^{-5} in p_y . Since this is

TABLE IV
Errors in the Pressure for the Forced Flow Test Problem When Different Boundary Extrapolations Are Used

		Errors in the pressure			
		192 × 192	256 × 256	384 × 384	Rate
Gauge	L_1	1.80e-3	1.88e-3	1.63e-3	0.35
	L_∞	1.18e-2	1.14e-2	9.44e-3	0.47
PmI	L_1	1.96e-3	1.13e-3	5.21e-4	1.91
	L_∞	2.09e-2	1.46e-2	9.11e-3	1.16
PmII	L_1	6.43e-4	3.47e-4	1.48e-4	2.10
	L_∞	4.92e-3	2.69e-3	1.17e-3	2.05
PmIII	L_1	5.69e-2	4.33e-2	2.92e-2	0.97
	L_∞	3.01e-1	2.30e-1	1.56e-1	0.96

Note. The rates were computed from the errors in the 256 × 256 and 384 × 384 grids.

TABLE V
Errors in the u -Component of Velocity for the Unforced Flow Test Problem

		Errors in the u velocity			
		96 \times 96	128 \times 128	192 \times 192	Rate
Gauge	L_1	1.06e-4	5.96e-5	2.64e-5	2.02
	L_∞	3.67e-4	2.06e-4	9.05e-5	2.03
PmI	L_1	6.91e-5	3.88e-5	1.71e-5	2.03
	L_∞	3.38e-4	1.90e-4	8.31e-5	2.04
PmII	L_1	6.90e-5	3.88e-5	1.70e-5	2.03
	L_∞	3.34e-4	1.87e-4	8.19e-5	2.04
PmIII	L_1	9.33e-5	5.48e-5	2.56e-5	1.88
	L_∞	3.59e-4	2.08e-4	9.53e-5	1.93

significantly smaller than the estimated errors used to compute the convergence rates, using the reference solution is justified. It should be noted that the standard Richardson extrapolation techniques commonly employed to estimate convergence rates can be misleading in this context. In particular, the pressure gradient computed with projection method I will appear to converge quite nicely at the boundary if only a Richardson procedure is used. In this case, the pressure gradient is converging to the solution of a different equation.

For each method, a solution is computed on 96 \times 96, 128 \times 128, and 192 \times 192 grids, and convergence rates are again computed in the L_1 and L_∞ norms using the 96 \times 96 and 192 \times 192 grids. The viscosity is set to $\nu = 1/16$. Since the flow is not forced except by the motion of the top wall, the magnitude of the v -component of the velocity decays rapidly while that of the u -component increases throughout the run at the top wall. The errors are estimated at time 0.25 in the u -component of the velocity and the pressure when the maximum value of u is about 0.86, while the maximum of v has dropped to about 0.39. The time step used is $\Delta t = 0.5h$.

Table V shows the estimated error and convergence rates for the u -velocity in this problem while the values for the pressure appear in Table VI.

- The gauge method displays fully second-order accuracy in both the velocity and the pressure as in the first example.

TABLE VI
Errors in the Pressure for the Unforced Flow Test Problem

		Errors in the pressure			
		96 \times 96	128 \times 128	192 \times 192	Rate
Gauge	L_1	6.89e-5	3.87e-5	1.72e-5	2.02
	L_∞	3.37e-4	1.82e-4	7.77e-5	2.13
PmI	L_1	3.82e-5	2.17e-5	9.65e-6	2.00
	L_∞	1.91e-4	1.53e-4	1.16e-4	0.73
PmII	L_1	3.92e-5	2.18e-5	9.47e-6	2.07
	L_∞	1.83e-4	1.01e-4	4.34e-5	2.09
PmIII	L_1	7.43e-5	4.35e-5	2.03e-5	1.88
	L_∞	1.55e-3	1.10e-3	6.67e-4	1.23

- Projection method I displays second-order accuracy in the velocity but only first-order accuracy in the pressure. As in the first example, the error in the pressure is in the form of a boundary layer.
- Projection method II displays fully second-order accuracy in both the velocity and the pressure as in the first example.
- Unlike the first example, projection method III shows a decrease in the convergence rate for the pressure when measured in the L_∞ norm. The cause of this is investigated in the following section.

6.4. A Different Boundary Condition for Projection Method III

It is somewhat surprising that projection method III does not obtain full second-order accuracy for the unforced problem. Some understanding of the cause of the lack of accuracy can be gained by considering the discrete divergence of the computed velocity. Since an approximate projection is being used, the discrete divergence of \mathbf{u}^n will not be zero for any of the methods. The L_1 and L_∞ norm of the discrete divergence of \mathbf{u}^n computed with centered differences at time 0.25 is shown for each method in Table VII. Two pertinent points can be made based on the data. First, projection method II has substantially less error in the divergence of \mathbf{u}^n than the other methods, and this error appears to be converging to zero at a higher rate than the other methods. On the other hand, projection method III has a first-order error in the divergence of \mathbf{u}^n .

The cause of this problem can be traced to the normal boundary condition for \mathbf{u}^* . Although the normal mode analysis indicates that this boundary condition can be chosen arbitrarily subject to the constraint (10), the choice of boundary condition will certainly affect the character of \mathbf{u}^* near the boundary. Given the evolution equation for \mathbf{u}^* in PmIII, \mathbf{u}^* is not a close approximation to \mathbf{u}^{n+1} , so choosing $\hat{\mathbf{n}} \cdot \mathbf{u}^* = \hat{\mathbf{n}} \cdot \mathbf{u}_b^{n+1} = 0$ for this problem causes $\nabla \cdot \mathbf{u}^*$ to be large near the boundary. A surface plot of $\nabla \cdot \mathbf{u}^*$ from the 96×96 run at time 0.125 is displayed in Fig. 2 and clearly shows a pronounced boundary layer.

Recall the relationship between ϕ and p given in Eq. (76). Using the definition of ϕ from Eqs. (71) and (72), this can be written as

$$\nabla_h p^{n+1/2} = \frac{\nabla_h \phi^{n+1}}{\Delta t} - \frac{\nu}{2} \nabla_h \nabla_h \cdot \mathbf{u}^*. \tag{77}$$

TABLE VII
Errors in the Divergence of \mathbf{u}^n for the Unforced Flow Test Problem

		Divergence errors			
		96 × 96	128 × 128	192 × 192	Rate
Gauge	L_1	1.11e-3	6.22e-4	2.75e-4	2.01
	L_∞	3.64e-3	2.05e-3	9.12e-4	2.00
PmI	L_1	2.30e-5	1.26e-5	5.52e-6	2.05
	L_∞	7.99e-4	5.96e-4	3.95e-4	1.01
PmII	L_1	9.38e-6	4.30e-6	1.42e-6	2.72
	L_∞	2.25e-4	1.33e-4	6.10e-5	1.88
PmIII	L_1	5.20e-4	3.20e-4	1.58e-4	1.71
	L_∞	1.19e-2	9.28e-3	5.30e-3	1.16

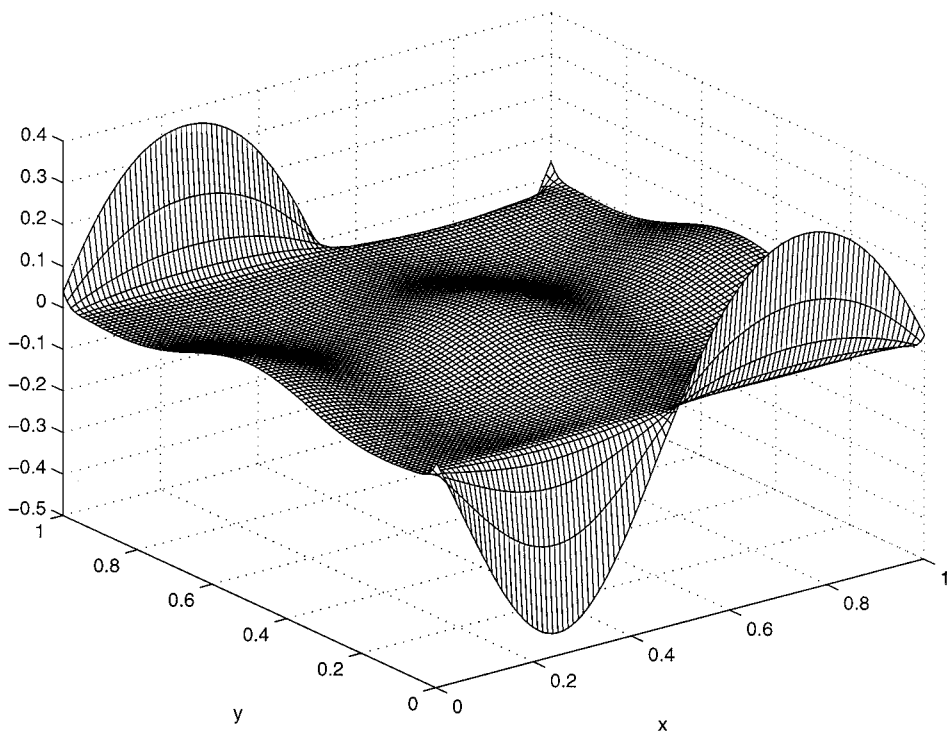
Div \mathbf{U}^* - Time = 0.125

FIG. 2. Surface plot of $\nabla \cdot \mathbf{u}^*$ for projection method III at time 0.125. Note the pronounced boundary layer.

Hence, the accuracy of the pressure depends on the behavior of $\nabla_h \cdot \mathbf{u}^*$. For this problem, the sharp boundary layer in $\nabla_h \cdot \mathbf{u}^*$ directly affects the accuracy of the pressure.

Following this reasoning, it should be the case that a boundary condition for $\hat{\mathbf{n}} \cdot \mathbf{u}^*$ which eliminates the boundary layer in $\nabla_h \cdot \mathbf{u}^*$ should also eliminate the error in the pressure. To test this hypothesis, the unforced problem was run again using a different boundary condition. Instead of restricting \mathbf{u}^* at the boundary with a Dirichlet condition, values at the boundaries are required to satisfy an extrapolation condition. Specifically, the value at the lower wall, $v_{i,0}^*$, must satisfy the “free” boundary condition

$$v_{i,0}^* - 3v_{i,1}^* + 3v_{i,2}^* - v_{i,3}^* = 0,$$

with the obvious counterpart at the top wall. This condition can also be interpreted as an approximation to $\frac{\partial^3}{\partial y^3} v^* = 0$.

Figure 3 displays $\nabla \cdot \mathbf{u}^*$ at time 0.125 using the free boundary condition. The size of the boundary layer has decreased an order of magnitude to the size of that in the interior. Convergence results using this new boundary condition are shown in Table VIII. It is clear from the results that the divergence of \mathbf{u}^* has also been reduced dramatically and is converging to zero at a rate higher than expected (as in PmII for this problem). Also, the first-order error in the pressure has been improved to second-order as expected.

The above boundary condition would certainly be more complicated to implement in the presence of complex geometries and hence may be less desirable in practice. The point to

Div \mathbf{U}^* - Time =0.125

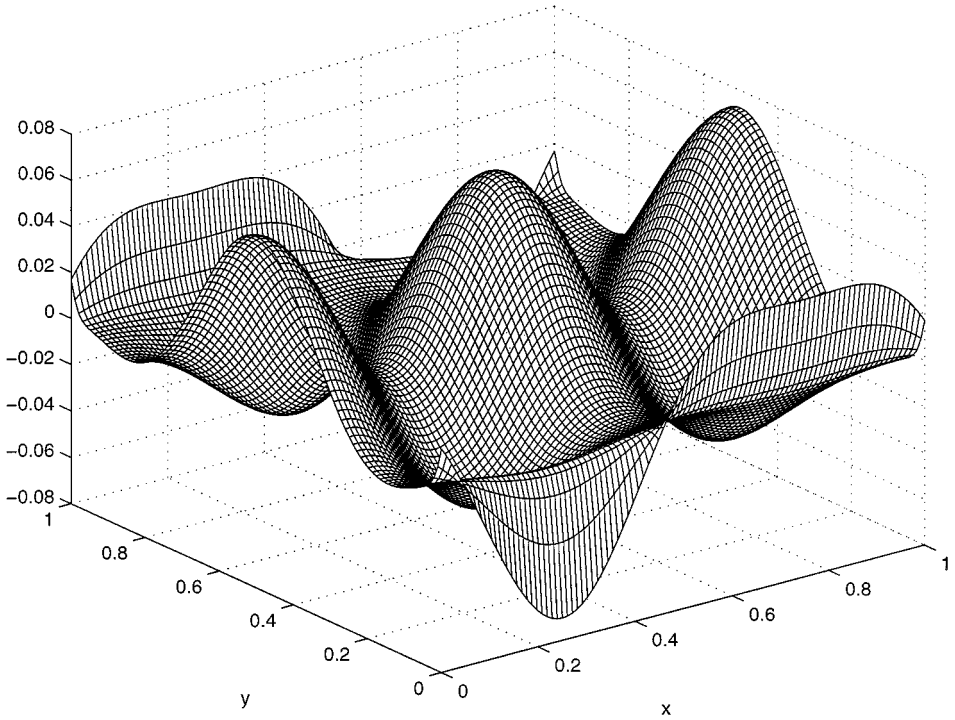


FIG. 3. Surface plot of $\nabla \cdot \mathbf{u}^*$ for projection method III with the free boundary condition. The boundary layer has been dramatically reduced.

be made is that although the normal boundary condition for \mathbf{u}^* is mathematically arbitrary, the choice can affect the accuracy of the numerical solution.

6.5. Smoothness of the Pressure Error

Despite the fact that projection methods II and III display optimal convergence rates in the pressure, the pressure error is not a completely smooth function near the solid wall boundaries. Figure 4 displays profiles of the pressure error near the top boundary. Despite

TABLE VIII
Errors in the Unforced Flow Test Problem for Projection Method III
Using the Free Boundary Condition

Errors for PmIII with modified boundary value					
		96 × 96	128 × 128	192 × 192	Rate
u	L_1	6.96e-5	3.91e-5	1.72e-5	2.03
	L_∞	3.21e-4	1.81e-4	8.01e-5	2.02
p	L_1	3.75e-5	2.12e-5	9.37e-6	2.02
	L_∞	1.58e-4	9.17e-5	4.22e-5	1.92
div	L_1	9.31e-5	4.32e-5	1.46e-5	2.67
	L_∞	1.80e-3	1.08e-3	5.10e-4	1.82

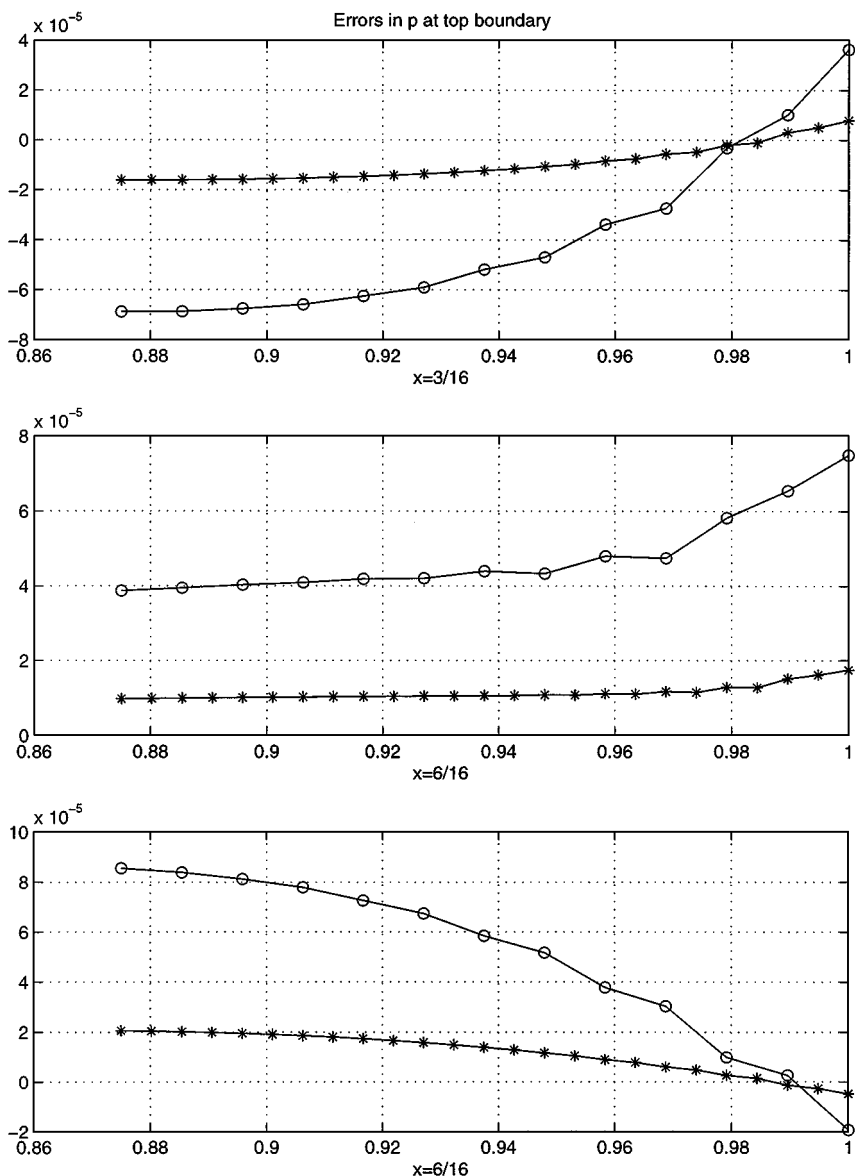


FIG. 4. Error in the pressure for the projection method II on the unforced problem. The three graphs correspond to profiles at x locations $3/16$, $6/16$, and $9/16$. Each graph shows the error from the 96×96 (\circ) and 192×192 ($*$) runs.

the slightly irregular shape of the error, the overall size is still converging to zero at a second-order rate.

The lack of smoothness in the pressure can be better observed by examining the error in p_y , the component of the pressure gradient normal to the boundary at $y = 1$. Figure 5 displays profiles of the error in p_y near the top boundary. The slight irregularities in the pressure error create noticeable irregularities in the error of p_y .

Table IX displays the errors and convergence rates for p_y for the unforced flow problem. Several comments can be made based on the data.

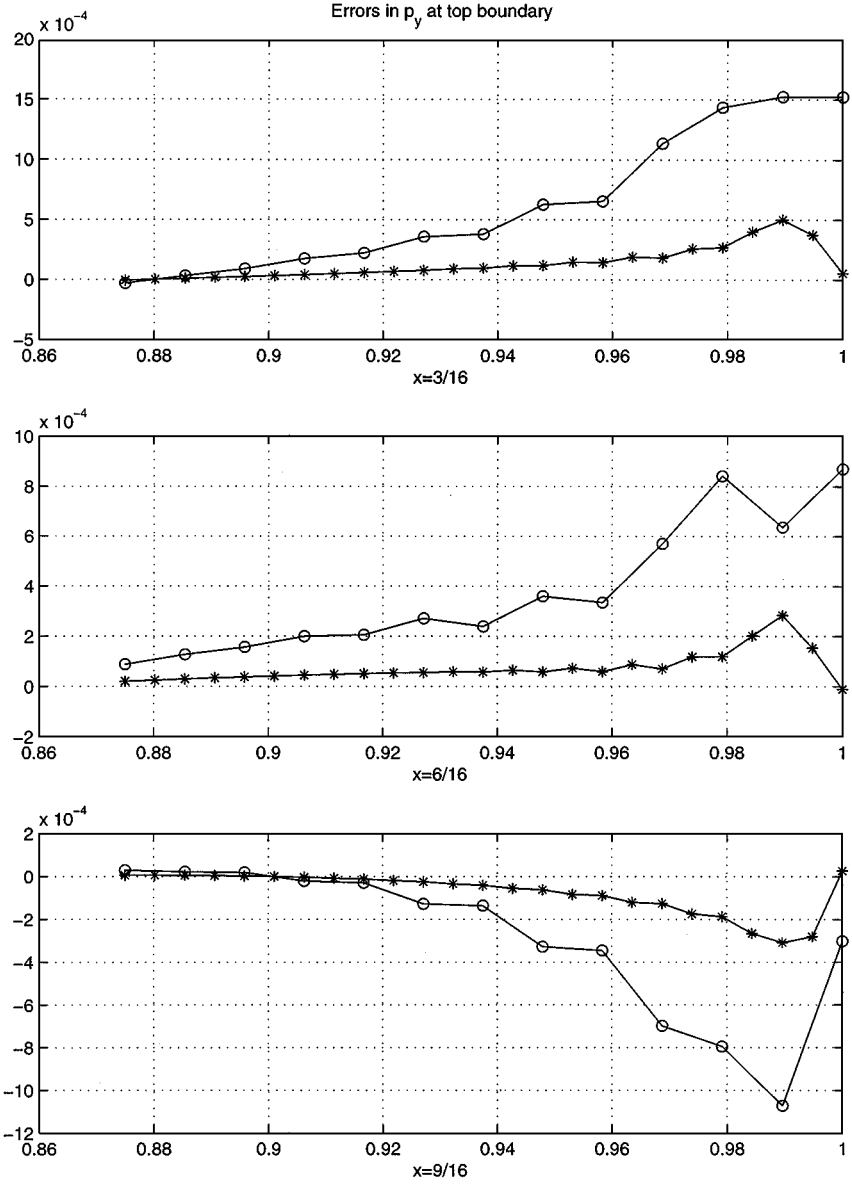


FIG. 5. Error in the p_y for the projection method II on the unforced problem. The three graphs correspond to profiles at x locations 3/16, 6/16, and 9/16. Each graph shows the error from the 96×96 (o) and 192×192 (*) runs.

- The gauge method displays fully second-order convergence in p_y .
- Projection method I displays zeroth-order convergence of p_y in the L_∞ norm since p_y at the boundaries is not allowed to change by the pressure-update equation.
- Both projection methods II and III show fully second-order accuracy for the pressure gradient measured in the L_1 norm. (Note that PmIII was computed using the modified boundary condition for $\hat{\mathbf{n}} \cdot \mathbf{u}^*$.)
- Both projection methods II and III show a decrease in the observed convergence rate for the pressure gradient measured in the L_∞ norm.

TABLE IX
Errors in p_y for the Unforced Flow Test Problem

		Errors in p_y			
		96 × 96	128 × 128	192 × 192	Rate
Gauge	L_1	7.06e-4	3.86e-4	1.66e-4	2.10
	L_∞	8.79e-3	4.86e-3	2.12e-3	2.07
PmI	L_1	9.76e-4	7.32e-4	4.85e-4	1.02
	L_∞	4.37e-2	4.65e-2	4.90e-2	-0.17
PmII	L_1	3.43e-4	1.87e-4	8.06e-5	2.10
	L_∞	2.01e-3	1.29e-3	6.90e-4	1.55
PmIII	L_1	4.47e-4	2.44e-4	1.05e-4	2.10
	L_∞	5.52e-3	3.83e-3	2.26e-3	1.30

The cause of the slightly lower convergence rates for the p_y can again be traced to the lack of smoothness of the Laplacian term in the pressure-update Eq. (74). The fact that the pressure itself is converging at the optimal rate indicates that the drop in convergence rates for the gradient is caused by spatial rather than temporal error. Depending on the implementation, the error in the pressure gradient due to a lack of smoothness in the pressure correction terms could potentially be exacerbated by the presence of complex geometries.

7. CONCLUSIONS

The class of incremental pressure projection methods discussed in this paper is characterized by the choice of three ingredients: the approximation to the pressure gradient term in the momentum equation, the formula used for the global pressure update during the time step, and the boundary conditions. We have shown how the three ingredients are coupled and how they can be combined to yield a fully second-order numerical method.

The boundary conditions one chooses for the intermediate field \mathbf{u}^* must result in a second-order approximation to $\mathbf{u}^{n+1}|_{\partial\Omega} = \mathbf{u}_b^{n+1}$. If the conditions for \mathbf{u}^* are separated into normal and tangential components, there is apparently some freedom in choosing the normal component since the required boundary condition for the potential ϕ in the projection step can be adjusted to ensure that $\hat{\mathbf{n}} \cdot \mathbf{u}^{n+1}|_{\partial\Omega} = \hat{\mathbf{n}} \cdot \mathbf{u}_b^{n+1}$. However, as demonstrated by the numerical experiments with PmIII, the choice of the normal boundary condition can affect the smoothness of \mathbf{u}^* near the boundary and therefore can also play a role in the accuracy with which the pressure is recovered. On the other hand, the tangential component of \mathbf{u}^* at the boundary cannot be set to an arbitrary value. Instead, it must be chosen in a manner which ensures that $\hat{\boldsymbol{\tau}} \cdot (\mathbf{u}^* - \nabla\phi^{n+1})|_{\partial\Omega} = \hat{\boldsymbol{\tau}} \cdot \mathbf{u}_b^{n+1}$ is approximately satisfied. This can be accomplished by approximating $\nabla\phi^{n+1}$, and the accuracy necessary in this approximation differs from method to method.

The methods of Bell, Colella, and Glaz and PmI approximate the pressure gradient in the momentum equation with a lagged value from the previous time step and use a pressure-update formula which is clearly not consistent with a high-order discretization of the Navier–Stokes equations. Despite this inconsistency, the time-discrete normal mode analysis of the unsteady Stokes equations shows these methods are second-order accurate in the velocities even if the approximation to $\nabla\phi^{n+1}$ in the tangential boundary condition

for \mathbf{u}^* is neglected. However, the inconsistency in the pressure-update formula results in a first-order error in the pressure which appears as a boundary layer in the numerical results presented.

The analysis demonstrates that a simple modification to the pressure-update formula, given by Eq. (13), yields a method which is second-order accurate in both the velocities and the pressure (PmII). This becomes critically important in applications in which stresses or other pressure-dependent quantities must be computed at solid walls. In addition, the tables displaying numerical results for the velocities and the pressure indicated that the errors for PmII are smaller than the errors of the other methods.

Methods similar to PmIII and that of Kim and Moin completely eliminate the pressure gradient term from the momentum equation. As a result, \mathbf{u}^* is only a first-order approximation to the velocity at the end of the time step. Consequently $\nabla\phi^{n+1}$ is $\mathcal{O}(\Delta t)$, which cannot be neglected in the tangential boundary condition for \mathbf{u}^* . The normal mode analysis shows that using a lagged value of ϕ , i.e., $\hat{\tau} \cdot (\mathbf{u}^* - \nabla\phi^n)|_{\partial\Omega} = \hat{\tau} \cdot \mathbf{u}_b^{n+1}$, is sufficient to achieve second-order accuracy. Despite the apparent freedom in choosing the normal boundary condition for \mathbf{u}^* , the numerical results performed on the full Navier–Stokes equations reveal that PmIII suffers from a decrease in accuracy of the pressure near the boundary when $\hat{\mathbf{n}} \cdot \mathbf{u}^* = \hat{\mathbf{n}} \cdot \mathbf{u}_b^{n+1}$ is used as a boundary condition. Because the computation of the pressure in this method depends indirectly on $\nabla \cdot \mathbf{u}^*$, the choice of boundary condition for \mathbf{u}^* is important in obtaining an accurate approximation for p . Numerical tests suggest that the boundary condition for \mathbf{u}^* should be chosen to keep $\nabla \cdot \mathbf{u}^*$ from developing large gradients near the boundary. One such boundary condition is suggested and shown to restore second-order accuracy in the pressure.

A gauge method that also eliminates the pressure gradient term from the momentum equation was analyzed as well. The gauge method variable \mathbf{m} (equivalent to \mathbf{u}^* during the first time step) is not discarded but used throughout the computation. This usually implies that the difference between \mathbf{m}^n and the fluid velocity \mathbf{u}^n becomes $\mathcal{O}(1)$, requiring extrapolation in time of ϕ in the tangential boundary condition for \mathbf{m}^{n+1} in order to achieve second-order accuracy. All numerical tests confirm this result. One can think of the gauge method as a generalization of the projection method. If the variable \mathbf{m} is kept throughout the computation, the result is the gauge method. However, if \mathbf{m} is reset to \mathbf{u} at the end of each time step, the result is a projection method. More generally, one could reset \mathbf{m} to \mathbf{u} after a number of time steps. It is still an open and interesting question whether there are any significant advantages in using gauge method variables in finite difference methods for incompressible flow.

Several comments should be made concerning the accuracy of the pressure in numerical computations. Quite often, semi-implicit projection methods are applied to problems in which the viscosity is small. Since the predicted first-order errors in the pressure are scaled by ν , it is not clear whether the improved pressure-update formula is beneficial in such situations. Also, the numerical examples presented here were set in a simple computational domain, and it is possible that there are additional issues to be addressed in cases where solid wall boundaries contain corners or other features. Finally, in some applications of projection methods, second-order accuracy in the pressure may not be relevant or in some cases even possible due to the treatment of other terms in the equations (e.g., [11, 31]).

The major contributions of this paper are a better understanding of the order of convergence of certain projection methods, simple modifications to existing methods that eliminate first-order errors in the computed pressure near solid boundaries, and an explanation of the

relationship between boundary conditions for intermediate quantities and the accuracy in the pressure. In applications where an accurate representation of the pressure near solid wall boundaries is required, the results in this paper provide an important improvement in accuracy for a popular class of projection methods.

ACKNOWLEDGMENT

The authors thank W. Henshaw for many useful discussions during the development of this paper.

REFERENCES

1. A. S. Almgren, J. B. Bell, P. Colella, and L. H. Howell, Adaptive projection method for the incompressible Euler equations, in *Proceedings of the Eleventh AIAA Computational Fluid Dynamics Conference, AIAA, June 1993*, p. 530.
2. A. S. Almgren, J. B. Bell, and W. Y. Crutchfield, Approximate projection methods. 1. Inviscid analysis, *SIAM J. Sci. Comput.* **22**(4), (2000).
3. A. S. Almgren, J. B. Bell, and W. G. Szymczak, A numerical method for the incompressible Navier–Stokes equations based on an approximate projection, *SIAM J. Sci. Comput.* **17**(2), (1996).
4. A. S. Almgren, J. B. Bell, and W. G. Szymczak, A numerical method for the incompressible Navier–Stokes equations based on an approximate projection, *SIAM J. Sci. Comput.* **17** (1996).
5. J. B. Bell, P. Colella, and H. M. Glaz, A second order projection method for the incompressible Navier–Stokes equations, *J. Comput. Phys.* **85**, 257 (1989).
6. J. B. Bell, P. Colella, and L. H. Howell, An efficient second-order projection method for viscous incompressible flow, in *Proceedings of the Tenth AIAA Computational Fluid Dynamics Conference, AIAA, June 1991*, p. 360.
7. O. Botella, On the solution of the Navier–Stokes equations using Chebyshev projection schemes with third-order accuracy in time, *Computers Fluids* **26**, 107 (1997).
8. T. F. Buttké, Velocity methods: Lagrangian numerical methods which preserve the Hamiltonian structure of incompressible fluid flow, in *Vortex Flows and Related Numerical Methods*, edited by J. T. Beale, G.-H. Cottet, and S. Huberson (Kluwer Academic, Dordrecht/Norwell, MA, 1993), p. 39. [NATO ASI Series C, Vol. 395.]
9. A. J. Chorin, Numerical solution of the Navier–Stokes equations, *Math. Comput.* **22**, 745 (1968).
10. A. J. Chorin, On the convergence of discrete approximations to the Navier–Stokes equations, *Math. Comput.* **23**, 341 (1969).
11. P. Colella and D. P. Trebotich, Numerical simulation of incompressible viscous flow in deforming domains, *Proc. Nat. Acad. Sci. USA* **96** (1999).
12. R. Cortez, *Impulse-Based Particle Methods for Fluid Flow*, Ph.D. thesis, University of California, Berkeley, May 1995.
13. R. Cortez, An impulse-based approximation of fluid motion due to boundary forces, *J. Comput. Phys.* **123**, 341 (1996).
14. W. E and J. Guo Liu, Projection method. I. Convergence and numerical boundary layers, *SIAM J. Numer. Anal.* **32**, 1017 (1995).
15. W. E and J. Guo Liu, *Gauge Method for Viscous Incompressible Flows*, unpublished, 1996.
16. W. E and J. Guo Liu, Projection method II. Godunov–Ryabenki analysis, *SIAM J. Numer. Anal.* **33**, 1597 (1996).
17. W. E and J. Guo Liu, Finite difference schemes for incompressible flows in the velocity-impulse density formulation, *J. Comput. Phys.* **130**, 67 (1997).
18. K. Goda, A multistep technique with implicit difference schemes for calculating two- or three-dimensional cavity flows, *J. Comput. Phys.* **30**, 76 (1979).
19. W. D. Henshaw, A fourth-order accurate method for the incompressible Navier–Stokes equations on overlapping grids, *J. Comput. Phys.* **113**, 13 (1994).

20. W. D. Henshaw and H.-O. Kreiss, Analysis of a difference approximation for the incompressible Navier–Stokes equations, Research Report LA–UR–95–3536, Los Alamos National Laboratory, 1995.
21. W. D. Henshaw, H.-O. Kreiss, and L. Reyna, A fourth-order accurate difference approximation for the incompressible Navier–Stokes equations, *Computers Fluids* **23**, 575 (1994).
22. S. Hugues and A. Randriamampianina, An improved projection scheme applied to pseudospectral methods for the incompressible Navier–Stokes equations, *J. Numer. Meth. Fluids* **28**, 501 (1998).
23. G. E. Karniadakis, M. Israeli, and S. A. Orszag, High-order splitting methods for the incompressible Navier–Stokes equations, *J. Comput. Phys.* **97**, 414 (1991).
24. J. Kim and P. Moin, Application of a fractional-step method to incompressible Navier–Stokes equations, *J. Comput. Phys.* **59**, 308 (1985).
25. M. F. Lai, *A Projection Method for Reacting Flow in the Zero Mach Number Limit*, Ph.D. thesis, University of California, Berkeley, 1993.
26. M. F. Lai, J. Bell, and P. Colella, A projection method for combustion in the zero Mach number limit, in *Proceedings of the Eleventh AIAA Computational Fluid Dynamics Conference, AIAA, June 1993*, p. 776.
27. M. L. Minion, A note on the stability of Godunov-projection methods, *J. Comput. Phys.* **123** (1996).
28. M. L. Minion, A projection method for locally refined grids, *J. Comput. Phys.* **127** (1996).
29. S. A. Orszag, M. Israeli, and M. O. Deville, *Boundary conditions for incompressible flows*, *J. Sci. Comput.* **1**, 75 (1986).
30. V. I. Oseledets, On a new way of writing the Navier–Stokes equation: The Hamiltonian formalism, *Comm. Moscow Math. Soc.* **44**, 210 (1989).
31. R. B. Pember, L. H. Howell, J. B. Bell, P. Colella, W. Y. Crutchfield, W. A. Fiveland, and J. P. Jesse, An adaptive projection method for unsteady low-Mach number combustion, *Comb. Sci. Tech.* **140**, 123 (1998).
32. J. B. Perot, An analysis of the fractional step method, *J. Comput. Phys.* **108**, 51 (1993).
33. R. Rannacher, *The Navier–Stokes Equations II: Theory and Numerical Methods*. Lecture Notes in Mathematics (Springer-Verlag, New York/Berlin, 1992, Vol. 1530).
34. M. C. Recchioni and G. Russo, Hamilton-based numerical methods for a fluid-membrane interaction in two and three dimensions, *SIAM J. Sci. Comput.* **19**, 861 (1998).
35. J. Shen, On error estimates of the projection methods for the Navier–Stokes equations: Second-order schemes, *Math. Comput.* **65**, 1039 (1996).
36. J. C. Strikwerda and Y. S. Lee, The accuracy of the fractional step method, *SIAM J. Numer. Anal.* **37**, 37 (1999).
37. D. M. Summers and A. J. Chorin, Numerical vorticity creation based on impulse conservation, *Proc. Nat. Acad. Sci. U.S.A.* **93**, 1881 (1996).
38. R. Temam, Remark on the pressure boundary condition for the projection method, *Theoret. Comput. Fluid Dynam.* **3**, 181 (1991).
39. J. Van Kan, A second-order accurate pressure-correction scheme for viscous incompressible flow, *SIAM J. Sci. Comput.* **7**, 870 (1986).
40. R. Verzicco and P. Orlandi, A finite-difference scheme for three-dimensional incompressible flows in cylindrical coordinates, *J. Comput. Phys.* **123**, 402 (1996).